ABSTRACT

Title of Thesis:	Analysis of Control Strategies for a Human Skeletal System Pedaling a Bicycle
Name of Candidate:	Scott Bradley Abbott
Degree and Year:	Master of Science, 1995
Thesis Advisor:	Professor William S. Levine Department of Electrical Engineering

The study of human locomotion has gained more attention recently with the availability of better analytic and computational tools with which to examine it. A subject under much study within the field today is the effort to model human motor control systems using control systems methods. Analytic, computational, and experimental studies of locomotion can produce models that provide further insight into the design and function of human systems, as well as provide directions for research into therapies for muscle and nerve related disorders affecting these systems.

This thesis examines how computational methods can be utilized to study the functionality of these systems. Building on past research, dynamic models for a human skeletal system pedaling a bicycle are used as a basis for examining various methods of implementing inputs that will control the cycling. Two models are used - a three degree-of-freedom model implementing ideal torque inputs at the hip, knees, and feet, and a one degree-of-freedom model involving

inputs at the hip and knee only. Both models are characterized by highly nonlinear dynamics, requiring the use of nonlinear analysis, optimization theory, and computational methods for examination. Control of the one degree-of-freedom model has been addressed in previous work; here, parameterization of the control and the process of learning it is examined. Next, control strategies for the more complex three degree-of-freedom model are developed. Finally, results for upright and recumbent cycling are compared using the three degree-of-freedom model.

ANALYSIS OF CONTROL STRATEGIES

FOR A HUMAN SKELETAL SYSTEM

PEDALING A BICYCLE

by

Scott Bradley Abbott

Thesis submitted to the Faculty of the Graduate School
of The University of Maryland in partial fulfillment
of the requirements for the degree of
Master of Science
1995

Advisory Committee:

Professor William S. Levine, Chairman/Advisor
Professor Fawzi Emad
Professor Andre Tits

ACKNOWLEDGMENTS

I wish to express my deep appreciation to my advisor, Professor William S. Levine, whose guidance, advice, and support were invaluable during my studies at the University of Maryland. His patience, modesty, and humor made it very easy to work with him, and his willingness to assist me was a strong element of my decision to complete my degree requirements. His intelligence and deep insights into the problems examined in this thesis contributed to each step of my progress and helped me to derive more benefit from this experience than I had thought possible.

I also wish to thank Professor Fawzi Emad and Professor Andre Tits for their efforts and time in reading my thesis and serving on my advisory committee, especially considering the short notice under which the committee was arranged.

Without the encouragement and support of my parents, Bonnie Abbott and Charles Abbott, I could not have come this far. They both passed away in the middle of this effort, and my depression following their passing nearly led me to quit. I deeply regret that they did not live to see me complete this degree, since it is as much their success as mine. However, I will always remember their belief in me, and I dedicate this work to them.

Finally, I wish to express my deep appreciation and love for my wife Athena, who instilled in me the belief that I could indeed finish, and who sacrificed tremendously for me. I hope that I can now repay her for all her love and support.

TABLE OF CONTENTS

LIST OF TABLES

LIST OF FIGURES

Chapter 1 The Study of Human Bicycling Models

1.1 Introduction

In this chapter, the physiological basis for the work in this thesis is discussed. Past experimentation on brain-muscle communication is discussed; a model for brain-muscle interaction is presented; and, the extent to which motor control is learnable is examined. Finally, the mathematical models used to study a skeletal system pedaling a bicycle are presented; the computational methods used are discussed; and, the results of this thesis are summarized.

1.2 Past and Present Research

The human body contains various types of control systems, including systems that control heart beat, body temperature, body weight, and eye movement. Leg motion is a system that is thought to not involve much conscious, voluntary intervention. To walk, most people do not have to concentrate consciously on moving the foot forward for each step; rather, it is a behavior that, once learned, can be "commanded" and executed with little thought. Similarly, once a cyclist learns to pedal a bicycle, the behavior can be repeated and adapted to changing conditions without much concentration on the part of the cyclist. Thus, the emphasis here is on motor control at a level below volition and cognition.

Pedaling a bicycle is a suitable candidate problem to examine, since it clearly contains elements of cognition in "commanding" the behavior and elements

of complex motor control. Additionally, it requires coordination of the motion of muscles and bones through the complicated three dimensional trajectories necessary to provide useful forward motion of the cycle (Ref. [2]).

Empirical data collected on this subject suggests a separation between cognitive functions and motor control. The mesencephalic cat experiment by Shik, Orlovsky, and Severin (Ref. [3]) demonstrated that walking could be induced in a cat with a severed mesencephelon through stimulation of the brain stem. The experiment and the resulting analysis showed that locomotion is controlled by neurons in the spinal cord and feedback from the periphery, as noted by Levine and Loeb in Reference 1, and is not necessarily a cognitive function.

This work is concerned with the dynamics and motor control aspects of pedaling a bicycle, and not with the cognitive aspect of commanding it. The problems to be examined include the development of signals that can achieve such coordination to accomplish successful pedaling, and parameterization of these signals. Experimental evidence has already shed some light on this approach by showing that the stimulation to the brain stem required to induce motion is a train of current pulses (Ref. [4]). But even if the structure of the signal is known, how is it realized? Is the mechanism for creating these signals intrinsically built into the body's circuitry, or is such a mechanism developed and tuned through direct experience?

Previous studies on bicycle pedaling have addressed the question of whether the process of acquisition of physical locomotive skills is "hard-wired" or is

"plastic (learnable)" (Ref. [1]). Early conjectural models tended toward the "hard wired" concept in modeling a motor program as a collection of parameters that, when received by the muscles, would initiate a specific action. However, experimental evidence has shown that locomotor-related neural circuits exhibit adaptive capacities (Ref. [4]), thus tending to the "plastic" model. Contemporary models of motor programs, such as the one proposed by Levine and Loeb in Reference 1, are collections of instructions which generate a variety of related movements. In fact, physiological models have come neural networks, which are systems whose parameters adjust over time and experience to meet the system's goals. Newell's work (1991, Ref. [5]) formulates the process of motor control behavior development in terms of solutions in a "perceptual-motor workspace".

Research into the pedaling problem by Levine, Zajac, et. al (Ref. [2]) has shown that the control to achieve maximal acceleration for a simple skeletal system is bang-bang. Further, it indicates that peripheral feedback adjusts the timing, not the shape, of the commands. Hence, there are several "levels" of control occurring between the brain and the muscles. A model proposed by Levine and Loeb (Ref. [1]) to account for this behavior is shown below in Figure 1.1.

We hypothesize that a pedaling subject is performing an action regulated not by cognitive brain functions, but by motor control parameters tuned by time and experience, as shown in Figure 1.1. Successful modeling of this motor control system can provide a map for parameterization of the signals required to perform the action, and a platform for studying how the acquisition of knowledge to perform

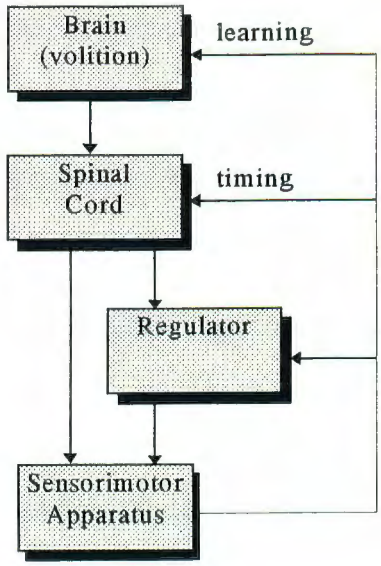

Figure 1.1: Motor Control Model (adapted from Ref. 1)

such tasks occurs. The benefit of such knowledge is clearly applicable to treatment of patients with motor control problems and to optimization of sports performance.

In summary, this work examines the signal patterns required to perform cycling and the parameterization of those signals. Cyclist "learning" is modeled as the process of solving optimization problems structured to model the acquisition of the parameters required to achieve successful pedaling. Additionally, the models are used to extract information useful to accomplishing successful pedaling. The dynamic models for bicycling used in this thesis are presented in the next section.

1.3 Cycling Models

There are two dynamic models of a two-legged human cycling system that are used to perform the analyses in this thesis, referred to here as the *Three Degree-of-Freedom* model and the *One Degree-of-Freedom* model. Both models are only

concerned with physical human geometry below the hip, with the assumption that the upper body is stationary. The One Degree-of-Freedom model is a reduction of the Three Degree-of-Freedom model in which the feet are ignored as input sources and are attached directly to the pedals. In all cases, the legs move in the same plane. The mathematical equations for both models were derived in Reference 6, sections 2.2 and 2.3.

1.3.1 Three Degree-of-Freedom Model

The geometry of the Three Degree-of-Freedom model is shown in Figure 1.2. The hip is kept fixed in the seat, and the upper body remains stationary. In Figure 1.2, H is the hip joint, K_l and K_r are the left and right knee joints respectively, A_l and A_r are the ankle joints, T_l and T_r are the toes, and B_l and B_r are the fixed points on the feet to which the pedals are attached. The point C marks the center of rotation of the crank. It is assumed that the right and left limbs are equivalent in length, size, and mass. We define P_1, P_2, P_3, P_4, and P_5 as the mass centers of the segments H_lK_l, K_lA_l, A_lB_l, B_lT_l, and B_lC. To parameterize this system, we define the following lengths:

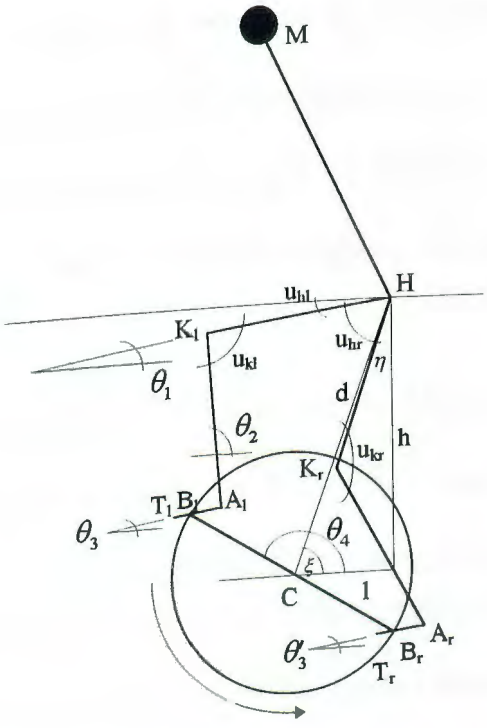

Figure 1.2: Three Degree-of-Freedom Cycling Model Geometry

$$l_1 = l_{11} + l_{12} = H_l P_1 + K_l P_1 = H_l K_l = H_r K_r$$
$$l_2 = l_{21} + l_{22} = K_l P_2 + A_l P_2 = K_l A_l = K_r A_r$$
$$l_3 = l_{31} + l_{32} = A_l P_3 + B_l P_3 = A_l B_l = A_r B_r$$
$$l_4 = l_{41} + l_{42} = B_l P_4 + T_l P_4 = B_l T_l = B_r T_r$$
$$l_5 = l_{51} + l_{52} = B_l P_5 + C P_5 = B_l C = B_r C$$

The left limb angles in the model are defined as follows:

θ_1 Hip Angle
θ_2 Calf Angle
θ_3 Ankle Angle
θ_4 Crank Angle

The right limb angles are denoted by θ'_n. In Reference 6, it is shown that θ_1 and θ_2 are functions of θ_3, θ'_3, and θ_4. Since we also include the assumption that the feet are fixed 180° apart in order to model "normal" cycling, then θ'_4 is merely $\theta_4 + \pi$.

Thus, this model has three degrees of freedom - θ_3 (the left ankle angle), θ'_3 (the right ankle angle), and θ_4 (the crank angle measured from horizontal to the left foot). The conventions for measuring the angles are discussed in Appendix A.

The dynamic equations for two-legged pedaling are highly nonlinear, and are expressed as follows

$$h_{11}\ddot{\theta}_3 + h_{12}\ddot{\theta}_4 + h_{14}\dot{\theta}_3^2 + h_{15}\dot{\theta}_4^2 + h_{15}\dot{\theta}_3\dot{\theta}_4 = -h_{16} + h_{17}u_{hl} + h_{18}u_{kl} + h_{19}u_{al}$$

$$h_{11}\ddot{\theta}'_3 + h_{12}\ddot{\theta}'_3 + h_{13}\dot{\theta}_3'^2 + h_{14}\dot{\theta}_4'^2 + h_{15}\dot{\theta}'_3\dot{\theta}'_4 = -h'_{16} + h'_{17}u_{hr} + h'_{18}u_{kr} + h'_{19}u_{ar}$$

$$\begin{aligned} &h_{21}\ddot{\theta}_3 + h'_{21}\ddot{\theta}'_3 + (h_{22} + h'_{22})\ddot{\theta}_4 + h_{23}\dot{\theta}_3^2 + h_{23}\dot{\theta}_3'^2 + (h_{24} + h'_{24})\dot{\theta}_4^2 + (h_{25} + h'_{25}\dot{\theta}'_3)\dot{\theta}_4 \\ &= h_{26} - h'_{26} + h_{27}u_{hl} + h'_{27}u_{hr} + h_{28}u_{kl} + h'_{28}u_{kr} + h_{29}u_{al} + h'_{29}u_{ar} - u_D \end{aligned}$$

The functions h_{ij}, i,j=1..9, are functions of the crank and ankle angles (although not of the velocity), and of the physical parameters of the cyclist. The input torques are defined as follows:

u_{al} Left Ankle Input
u_{ar} Right Ankle Input
u_{kl} Left Knee Input
u_{kr} Right Knee Input
u_{hl} Left Hip Input
u_{hr} Right Hip Input
u_D Resistance Torque

The physical parameters used for this simulation are listed in Appendix A.

1.3.2 One Degree-of-Freedom Model

The One Degree-of-Freedom cycling model is a reduced case of the Three Degree-of-Freedom model, and is shown in Figure 1.3. In the one Degree-of-

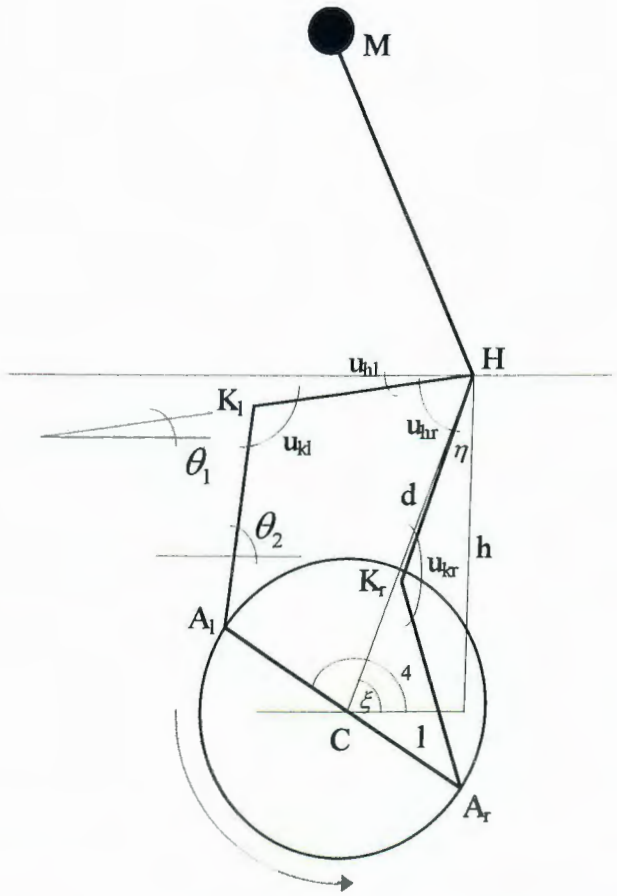

Figure 1.3: One Degree-of-Freedom Cycling Model Geometry

Freedom model, the ankles are fixed to the pedals, and thus the feet play no part in the dynamics. The ankle joints and the axis of rotation of the pedals effectively coincide. Since the feet don't play a role in pedaling the cycle, this model is only a one degree of freedom system. All other angles of the system are a function of θ_4, the crank angle, as shown in Reference 6. The dynamic equation representing two-legged pedaling is expressed in the following equation:

$$(h_1(\theta_4)+h_1(\theta_4+\pi))\ddot{\theta}_4-(h_2(\theta_4)+h_2(\theta_4+\pi))\dot{\theta}_4^2-(h_3(\theta_4)+h_3(\theta_4+\pi))$$
$$=h_4(\theta_4)u_{hl}+h_4(\theta_4+\pi)u_{hr}+h_5(\theta_4)u_{kl}+h_5(\theta_4+\pi)u_{kr}-u_D$$

where h_i, i=1..5 are defined in Reference 6, and are a function of θ_4 only.

1.4 Computational Methods

Computational simulations of the three degree-of-freedom model and the one degree-of-freedom model were performed using the mathematical software package MATLAB. To compute the trajectories of the dynamic equations, the function *ode23* was used to integrate the ordinary differential equations using second and third order Runge-Kutta algorithms. Several optimization problems were demonstrated using the *fmin* (unconstrained scalar optimization) and *fmins* (unconstrained optimization using simplex search algorithm) functions. The key MATLAB programs used are included in Appendix B.

1.5 Summary of Results

In Chapter 2, control of the one degree-of-freedom model is studied. In that chapter, it is demonstrated that successively complex cycling performance optimization problems can be formulated and solved, with successively better results. This serves as a model for learning locomotive behavior, in that the behavior is simple at first but can be improved through increasingly complex coordination of the limbs. In Chapter 3, control strategies for the three degree-of-freedom model are examined. The significant effects of the ankle angles on the rest of the model's dynamics lead to utilization of a fixed-ankle strategy. Through

analysis of the physical limits of the foot and analysis of the dynamic equations, regions are identified in which the foot should be constrained for effective cycling. Feedback linearization is used to show the ideal input torque profile for achieving a constant acceleration, and for identifying the ankle angle resulting in the minimal effort to complete a full cycle. Finally, in Chapter 4, results are developed for recumbent cycling and compared to upright cycling. Chapter 5 summarizes the work in this thesis, and presents suggestions for future extensions of this work.

Chapter 2 Analysis of the One Degree-of-Freedom Model

2.1 Introduction

In this chapter, control strategies for pedaling a bicycle as modeled by the One Degree-of-Freedom system presented in section 1.3.2 are examined. The response to both zero and nominal bang-bang input is presented. Chapter 1 develops an argument that locomotive behavior is learnable and can be parameterized; in this chapter, the process of learning effective cycling behavior is modeled through a series of increasingly complex optimization problems which identify the key parameters and provide some intuitive results.

2.2 Zero-Input Response

First, the response of the One Degree-of-Freedom model with zero input is examined. The zero-input response shows the effects of gravity on the system, and shows the minimum input magnitude required to overcome those effects. The zero input behavior of the One Degree-of-Freedom system was examined under the following initially stationary conditions:

$$\theta_4 \in [0, 2\pi]$$
$$\dot{\theta}_4(t_0) = 0$$
$$\ddot{\theta}_4(t_0) = 0$$
$$u_D = 0$$

where θ_4 is the cycle crank angle as shown in Figure 1.3. Except at two equilibrium points, any initial crank angle leads to a periodic acceleration in the

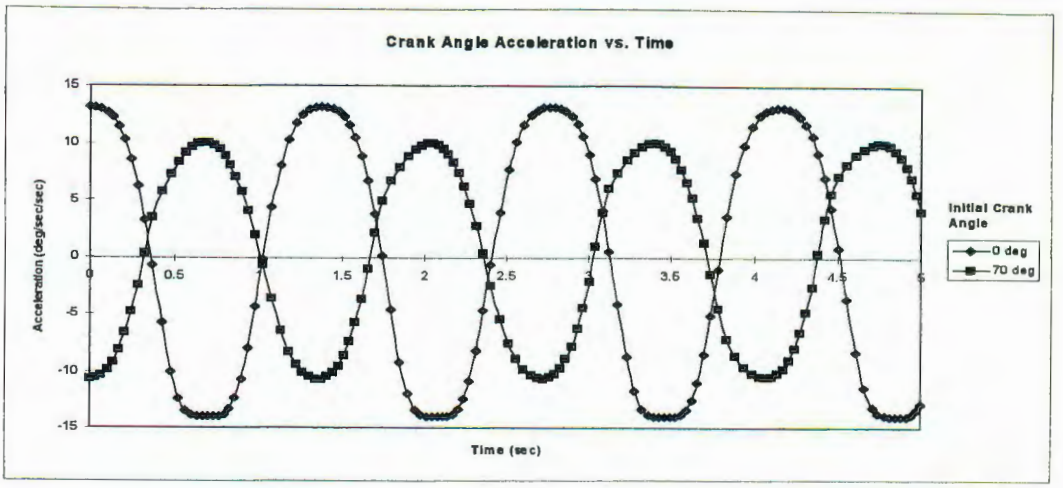

Figure 2.1: Crank Angle Acceleration, Frictionless system

absence of any friction, as shown in Figure 2.1. Consequently, the crank angle oscillates back and forth about its initial crank value. The farther the initial crank angle was from an equilibrium point, the greater the magnitude of the initial acceleration, and thus the greater the magnitude of the periodic acceleration. The equilibrium points can be found by realizing that for the given initial conditions, the model's dynamic equation (section 1.3.2) reduces to

$$\ddot{\theta}_4 = \frac{h_3(\theta_4) + h_3(\theta_4 + \pi)}{h_1(\theta_4) + h_1(\theta_4 + \pi)}$$

For the crank arm to remain stationary, the following relation must hold:

$$h_3(\theta_4) = h_3(\theta_4 + \pi)$$

and the crank angle θ_4 which solves this equation defines the equilibrium points. The solution to this equation is based solely on the geometric relationship between θ_1, θ_2, and θ_4. Since h_3 is the only term of the dynamics that accounts for gravity, [Ref. 6, eq. 2.3.21], the interpretation of an equilibrium point is a crank angle

position such that the legs and crank are balanced with respect to gravity. Any imbalance absent a forced input causes the crank to move toward the equilibrium angles. The acceleration profiles in Figure 2.1 were computed for a frictionless system; inclusion of a realistic non-zero friction term, particularly one which is a function of the crank velocity or acceleration, would obviously cause the acceleration to decay over time. Various types of friction can be represented through the friction term u_D, such as

Constant friction	α
Linear viscous damping	$\beta\dot{\theta}_4$
Air drag	$\gamma\dot{\theta}_4^2$
Flywheel inertia	$\delta\ddot{\theta}_4$

Appropriate values for the friction coefficients can be found in Reference 8. Figure 2.2 shows the equilibrium points versus the seat position for the parameter set detailed in Appendix A, where the seat position is defined by the angle ξ pictured in Figure 1.3. The plot labels above the curves in Figure 2.2 provide qualitative

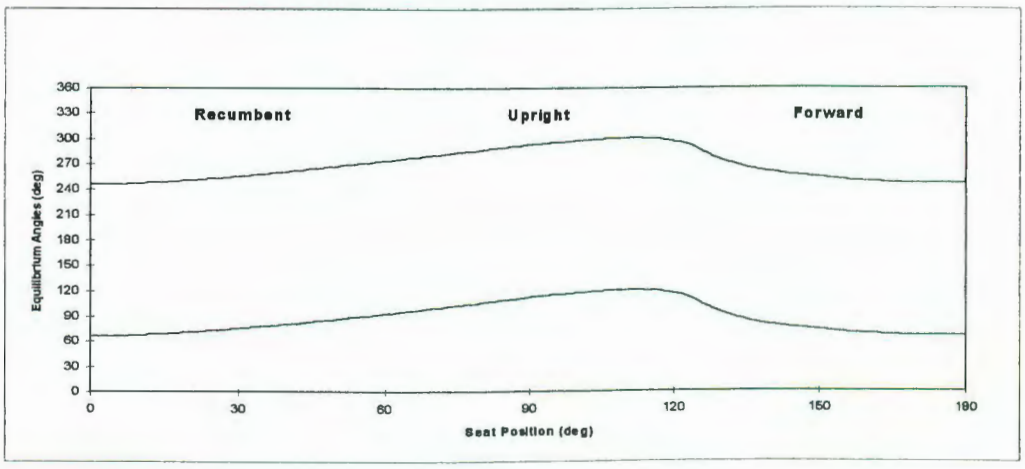

Figure 2.2: One Degree of Freedom Model Equilibria vs. Seat Position

descriptions of the position of the cyclist. The upright position is the normal position of a cyclist, seated above the crank center. In the recumbent position, the rider is seated behind the crank center (this position is utilized for several types of stationary exercise bicycles), and in the forward position, the rider is seated ahead of the crank center.

2.3 Bang-Bang Input Response

In Reference 6, Chapter 3, it was shown that the control which achieved a full rotation of the crank of the One Degree-of-Freedom system in minimum time consists of maximum extension torque at the hip between the minimum and maximum hip angle, a maximum flexion torque at the hip between the maximum and minimum hip angle, a maximum extension torque at the knee between the minimum and maximum knee angle, and a maximum flexion torque at the knee between the maximum and minimum knee angle[1]. This may be expressed more specifically as

$$u_{hl}(\theta_4) = \begin{cases} U_{hl_{\max}} & \text{for } \theta_{h_{\min}} \le \theta_4 \le \theta_{h_{\max}} \\ U_{hl_{\min}} & \text{for } \theta_{h_{\max}} \le \theta_4 \le \theta_{h_{\min}} \end{cases}$$

$$u_{hr}(\theta_4) = \begin{cases} U_{hr_{\min}} & \text{for } \theta_{h_{\min}} \le \theta_4 \le \theta_{h_{\max}} \\ U_{hr_{\max}} & \text{for } \theta_{h_{\max}} \le \theta_4 \le \theta_{h_{\min}} \end{cases}$$

$$u_{kl}(\theta_4) = \begin{cases} U_{kl_{\max}} & \text{for } \frac{\pi}{2} - \eta \le \theta_4 \le \frac{3\pi}{2} - \eta \\ U_{kl_{\min}} & \text{for } \frac{3\pi}{2} - \eta \le \theta_4 \le \frac{5\pi}{2} - \eta \end{cases}$$

$$u_{kr}(\theta_4) = \begin{cases} U_{kr_{\min}} & \text{for } \frac{\pi}{2} - \eta \le \theta_4 \le \frac{3\pi}{2} - \eta \\ U_{kr_{\max}} & \text{for } \frac{3\pi}{2} - \eta \le \theta_4 \le \frac{5\pi}{2} - \eta \end{cases}$$

---

[1] An update to the results in Reference 6 is shown in Appendix C.

where η is the hip-crank axis angle, and where

$$\theta_{h_{\max}} = \theta_4^* \left| \theta_1(\theta_4^*) > \theta_1(\theta_4) \;\; \forall \theta_4 \right.$$
$$\theta_{h_{\min}} = \theta_4^* \left| \theta_1(\theta_4^*) < \theta_1(\theta_4) \;\; \forall \theta_4 \right.$$

and where the inputs are bounded, i.e.

$$\exists U_{\max} \text{ constant, finite such that}$$
$$\left|U_{hl_{\max}}\right| \le U_{\max}, \quad \left|U_{kl_{\max}}\right| \le U_{\max}$$
$$\left|U_{hl_{\min}}\right| \le U_{\max}, \quad \left|U_{kl_{\min}}\right| \le U_{\max}$$
$$\left|U_{hr_{\max}}\right| \le U_{\max}, \quad \left|U_{kr_{\max}}\right| \le U_{\max}$$
$$\left|U_{hr_{\min}}\right| \le U_{\max}, \quad \left|U_{kr_{\min}}\right| \le U_{\max}$$

The left knee angle, defined as $\theta_1 + \pi - \theta_2$, reaches a minimum at $\frac{\pi}{2} - \eta$ and a maximum at $\frac{3\pi}{2} - \eta$ [Ref. 6, section 2.3]. A finite solution trajectory is guaranteed if the following constraint [Ref. 6, section 3.2] is met:

$$\left(h_3(\theta_4) + h_3(\theta_4 + \pi)\right) + h_4(\theta_4)u_{hl} + h_4(\theta_4 + \pi)u_{hr} + h_5(\theta_4)u_{kl} + h_5(\theta_4 + \pi)u_{kr} - u_D > 0 \;\; \forall \theta_4$$

An example of the acceleration profile with bang-bang input is provided in Figure 2.3. Simulations were configured to provide the inputs according to the conditions listed above. For small input magnitudes, the input was not enough to overcome the zero-input response of the system noted in the previous section, and thus full-rotation forward cycling was not achieved. This is in accordance with the condition 3.2.10 in Reference 6, which states that the input magnitude has to be enough to overcome the potential energy effects and resistance in order to induce forward cycling. However, once past the threshold, increasing input magnitudes

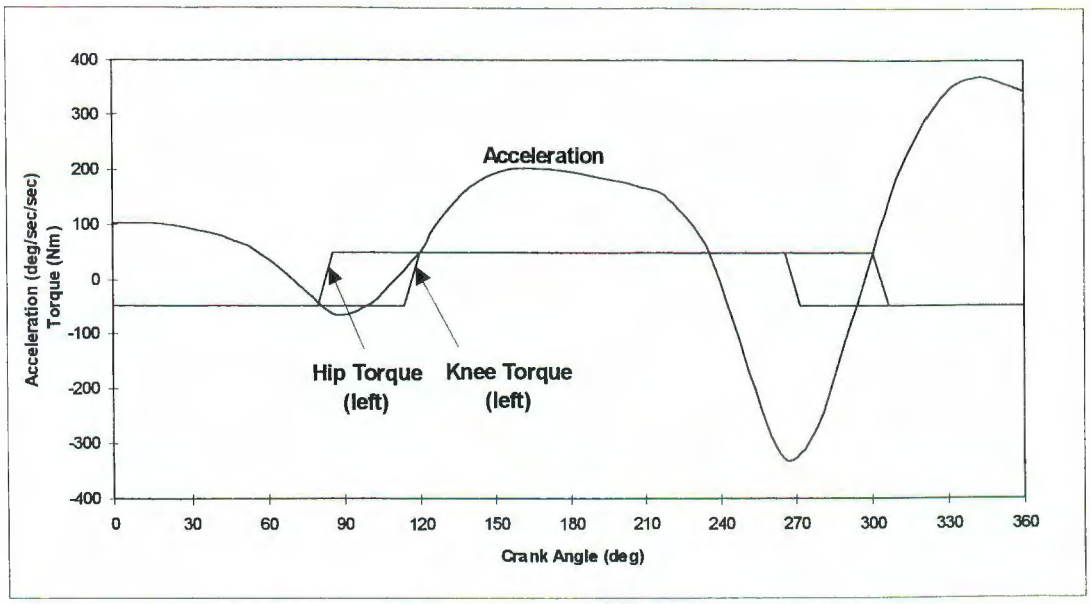

Figure 2.3: One Degree-of-Freedom Model Acceleration with Bang-Bang Input

resulted in increasingly faster full rotations of the crank angle. The joint torque magnitudes used for the remaining analysis in this chapter are listed in Appendix A.

2.4 Learning through Optimization

In this section, the results described so far for the One Degree-of-Freedom model are extended to simulate a human learning to pedal a bicycle. It has been established analytically that the input providing the minimum cycle time though one rotation of the crank is bang-bang, with the conditions mentioned in the previous section. Given this information, we hypothesize that the joint torques required to achieve minimal time cycling under similar but slightly different input conditions and constraints are bang-bang in nature. Thus, to model the learning process, the bang-bang conditions on the inputs are varied, and performance is optimized under

those conditions. For instance, if the input is constrained to change polarity only once, then the problem becomes finding the crank angle at which to execute the switch. Additionally, the hip and knee inputs can be constrained to switch polarity in a synchronized or unsynchronized fashion. Thus, the basic bang-bang profile of the input signal does not change, but the timing of the signal does. Formulating optimal control problems which arrive at solutions for timing the signals will model the tuning of the motor control mechanism by the spinal cord as pictured in Figure 1.1. If it can be shown that the problems which are formulated can be solved relatively easily, say with a simple gradient descent algorithm, then we hypothesize that such problems can be solved in reality - i.e. in the brain-spinal cord-muscle network. Simulation results show that performance improves as more complexity is added to the solution by allowing greater freedom in the input constraints. This series of problems models the human learning process in that cycling and other such complex activities may be achieved and optimized through refined, successive steps in coordination of the appropriate muscle groups and limbs.

2.4.1 Problem Formulation

The goal of the analysis is to minimize the following cost function:

$$J = \int_{t_0}^{t_f} dt = t_f - t_0$$

with the following boundary conditions

$$\theta_4(t_0) = \theta_{4_0}$$
$$\theta_4(t_f) = \theta_{4_0} + 2\pi$$
$$\dot{\theta}_4(t_0) > 0$$
$$\dot{\theta}_4(t_f) = \text{free}$$

The large number of parameters and complexity of the dynamics of the One Degree-of-Freedom model make an analytic solution difficult to find, but problems can be formulated to find numerical answers that provide insight into the solution.

Table 2.1: Extremal Angles of One Degree-of-Freedom Model

Angle	Value	at Crank Angle
min θ_1	13°	112°
max θ_1	60°	292°
min θ_2	105°	230°
max θ_2	147°	40°
min knee angle	62°	85°
max knee angle	126°	265°

For information, Table 2.1 shows the crank angles at which the joint extremal angles of the One Degree-of-Freedom model are attained for the parameters in Appendix A. The knee angle in Table 2.1 is defined to be $\theta_1 + \pi - \theta_2$.

2.4.2 Case 1: Minimum Cycle Time with One Synchronized Hip and Knee Switch

The analysis is begun with the simplest case possible - switching the polarity of the hip and knee torques only once per full rotation of the crank arm, and in a

synchronized manner. More specifically, the hip and knee inputs are bang-bang, can have only one of two values, and both are synchronized such that they switch values at the same crank angle. The goal is to minimize the time to complete one full cycle, as represented by the cost functional presented in the previous section. The following condition is put on both the hip and knee inputs:

$$u(\theta_4) = \begin{cases} U_1 \text{ for } \theta_4 \le \theta_s \\ U_2 \text{ for } \theta_4 > \theta_s \end{cases}$$

with $U_1 = - U_2$. Thus, the input profile will correspond to Figure 2.4.

A function computing cycle time based on the crank angle of the input polarity switch θ_s was minimized using a simplex search algorithm in MATLAB. With synchronized hip and knee inputs, the computational results for this particular problem, given the cyclist parameters in Appendix A, are listed in Table 2.2.

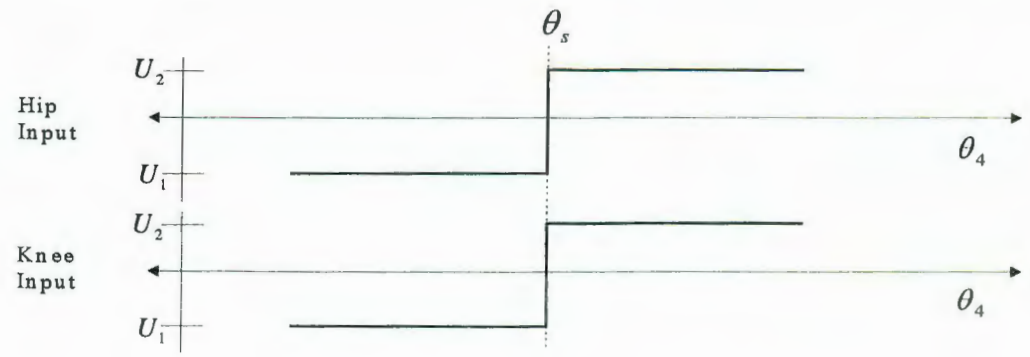

Figure 2.4: Input Schedule - Case 1

Table 2.2: Results for Case 1

	$\frac{\pi}{2} - \eta \le \theta_{4_0} \le \theta_{h_{min}}$	$\theta_{h_{max}} \le \theta_{4_0} \le \frac{3\pi}{2} - \eta$
Optimal switch angle θ_s	98°	278°
t_{cycle}	0.44 sec	0.44 sec

Multiple simulation runs show that the optimal switchpoints lie in the following ranges, given that the bang-bang input conditions listed in section 2.2 hold for the initial crank angle θ_{4_0}:

$$\theta_s \in \begin{cases} \left[\theta_{h_{\min}}, \frac{\pi}{2} - \eta\right] \text{ for } \theta_{h_{\max}} \le \theta_{4_0} \le \theta_{h_{\min}}, \theta_{h_{\min}} > \frac{\pi}{2} - \eta \\ \left[\frac{\pi}{2} - \eta, \theta_{h_{\min}}\right] \text{ for } \theta_{h_{\max}} \le \theta_{4_0} \le \theta_{h_{\min}}, \theta_{h_{\min}} < \frac{\pi}{2} - \eta \\ \left[\frac{3\pi}{2} - \eta, \theta_{h_{\max}}\right] \text{ for } \theta_{h_{\min}} \le \theta_{4_0} \le \theta_{h_{\max}}, \frac{3\pi}{2} - \eta > \theta_{h_{\max}} \\ \left[\theta_{h_{\max}}, \frac{3\pi}{2} - \eta\right] \text{ for } \theta_{h_{\min}} \le \theta_{4_0} \le \theta_{h_{\max}}, \frac{3\pi}{2} - \eta < \theta_{h_{\max}} \end{cases}$$

To summarize, the optimal switch angle occurred between the crank angle at which the minimum knee angle occurred, and the crank angle at which the minimum θ_1 (hip angle) occurred, thus compromising between the nominal bang-bang switchpoints for the hip and knee. It is easy to see why the optimal switch angle must lie in the region it does - by switching the input torques near first nominal bang-bang switchpoint the crank angle passes, the input closely follows the time minimal bang-bang optimal path for more than half of the rotation of the crank, rather than for only a small portion of the cycle.

2.4.3 Case 2: Minimum Cycle Time with One Unsynchronized Hip and Knee Switch

The next case is similar to the first, except that the hip and knee switch angles are now separated. The hip and knee input program is represented by:

$$u_{hip}(\theta_4) = \begin{cases} U_1 \text{ for } \theta_4 \le \theta_{s_{hip}} \\ U_2 \text{ for } \theta_4 > \theta_{s_{hip}} \end{cases}$$

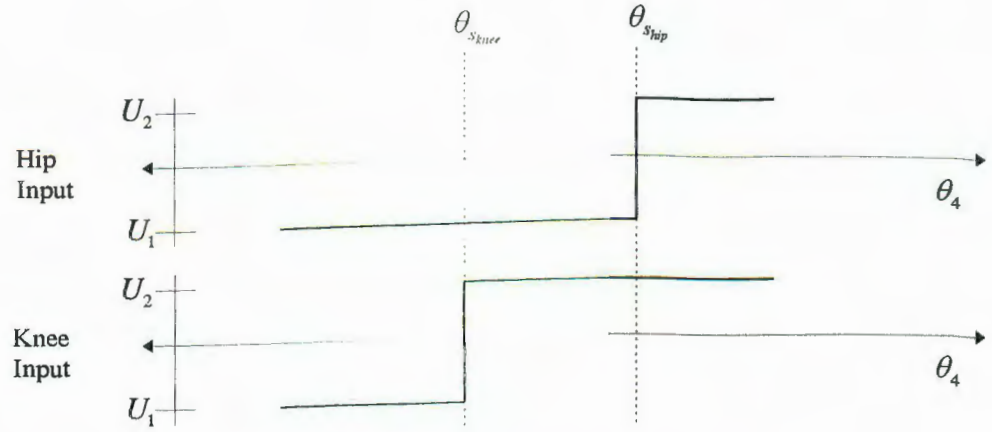

Figure 2.5: Input Schedule - Case 2

$$u_{knee}(\theta_4) = \begin{cases} U_1 \text{ for } \theta_4 \le \theta_{s_{knee}} \\ U_2 \text{ for } \theta_4 > \theta_{s_{knee}} \end{cases}$$

Thus, the input signals follow the profile shown in Figure 2.5.

With the knee and hip inputs decoupled and switched once during the single cycle, the computational results are presented in Table 2.3. The results show that the optimal switchpoints are given by the following expression:

$$\theta_{s_{knee}} = \begin{cases} \frac{\pi}{2} - \eta \text{ for } \frac{3\pi}{2} - \eta \le \theta_{4_0} \le \frac{\pi}{2} - \eta \\ \frac{3\pi}{2} - \eta \text{ for } \frac{\pi}{2} - \eta \le \theta_{4_0} \le \frac{3\pi}{2} - \eta \end{cases}$$

$$\theta_{s_{hip}} = \begin{cases} \theta_{h_{min}} \text{ for } \theta_{h_{min}} \le \theta_{4_0} \le \theta_{h_{max}} \\ \theta_{h_{max}} \text{ for } \theta_{h_{min}} \le \theta_{4_0} \le \theta_{h_{max}} \end{cases}$$

Table 2.3: Results for Case 2

	$\theta_{h_{max}} \le \theta_{4_0} \le \frac{\pi}{2} - \eta$	$\frac{\pi}{2} - \eta \le \theta_{4_0} \le \theta_{h_{max}}$	$\theta_{h_{min}} \le \theta_{4_0} \le \frac{3\pi}{2} -$	$\frac{3\pi}{2} - \eta \le \theta_{4_0} \le \theta_{h_{max}}$
$\theta_{s_{knee}}$	112°	112°	292°	292°
$\theta_{s_{hip}}$	85°	265°	265°	85°
t_{cycle}	0.435	0.432	0.431	0.434

Both switchpoints occurred close to the first nominal bang-bang switchpoints that the crank angle passed. The knee switch angle was close to the angle at which the knee angle was minimized. The hip input occurred close to the point at which the hip angle (θ_1) was minimized, indicating that the knee (as a point in space) had reached its maximal elevation, which is an intuitive result. Additionally, there was a slight improvement in the cycle time over Case 1, since both inputs were allowed to switch independently. The differences in cycle times in Table 2.3 are insignificant.

2.4.4 Case 3: Minimum Cycle Time with Two Unsynchronized Hip and Knee Switches

To further extend the problem, the input conditions were changed to allow two switches per cycle in both the hip and knee inputs, with the goal of further minimizing the time for one cycle. Specifically, the input schedule for the hip and knee inputs was changed to the following function characterized by two switch points each

$$u_{hip}(\theta) = \begin{cases} U_1 \text{ for } \theta < \theta_{s_{hip1}}, \theta > \theta_{s_{hip2}} \\ U_2 \text{ for } \theta_{s_{hip1}} \leq \theta \leq \theta_{s_{hip2}} \end{cases}$$

$$u_{knee}(\theta) = \begin{cases} U_1 \text{ for } \theta < \theta_{s_{knee1}}, \theta > \theta_{s_{knee2}} \\ U_2 \text{ for } \theta_{s_{knee1}} \leq \theta \leq \theta_{s_{knee2}} \end{cases}$$

Again, the assumption that U_1 and U_2 are the same in magnitude and opposite in sign remained. The computational results were as follows:

Table 2.4: Results for Case 3

$\theta_{s_{knee}}$	122°, 297°
$\theta_{s_{hip}}$	85°, 265°
t_{cycle}	0.420

and the resulting input schedule resembled that in Figure 2.6.

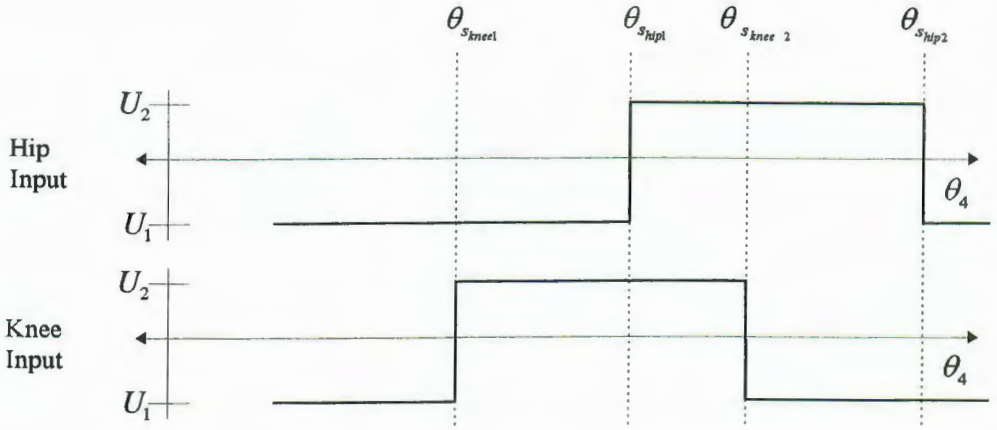

Figure 2.6: Input Schedule - Case 3

The addition of two more switchpoints into the problem helped to further reduce the cycle time. When the two hip and knee inputs were optimized independently, the knee switch angle stayed very close to the angle at which the knee angle was minimized or maximized. The hip inputs occurred very close to the points where the hip angle (θ_1) was minimized or maximized, indicating that the knee (as a point in space) had reached its maximal or minimal elevation. This is an intuitive result, in that little input effort is wasted by forcing a joint in the opposite direction of its current rotation. It also corresponds to the analytic results from Reference 6, Chapter 3, thereby computationally validating those results for this cycling model and set of cycling parameters.

2.5 Conclusions

In this chapter, several aspects of cycling have been studied through the use of the One Degree-of-Freedom model. First, given sufficient joint torque, effective forward rotation of the crank can be induced and analyzed with the One Degree-of-Freedom model. From analysis, it was found that the optimal control for minimum time cycling is bang-bang input at the hips and knees with switchpoints near joint angle extremals. Even if the input conditions are altered, the One Degree-of-Freedom model will find optimal bang-bang switchpoints at the angles defined by the analytic results; i.e. at the joint extremals. Through the formulation and solution of the optimal control problems for minimum time cycling, it was shown that the process of learning to pedal a bicycle can be modeled through a series of solutions to increasingly difficult problems. For example, it was shown that, given a bang-bang input profile for the joints, the cyclist can first learn where to pull up and push down the legs, and then learn to adjust the movement of the thighs and calves independently. Better performance - in this case a faster cycle time - is achieved through increasingly complex coordination of the limbs.

Chapter 3 Analysis of the Three Degree-of-Freedom System for Upright Cycling

3.1 Introduction

In this chapter, control strategies for cycling in the upright position using the Three Degree-of-Freedom model presented in Chapter 1 are examined. Upright cycling is examined first because it is the most common position for pedaling a bicycle. Again, this model is highly nonlinear and involves a large number of parameters, making utilization of analytical techniques difficult. In Reference 6, optimization of cycle time was not addressed due to the complexity introduced by the ankle angle dynamics. Here, analysis of control strategies for the Three Degree-of-Freedom model is approached from a computational perspective using a realistic set of parameters and constraints, and incorporating known behaviors.

The first step is to decouple the three equations composing the dynamics from the form in section 1.3.1, in order to provide a clearer expression for the behavior of the ankle angles and the crank angle. Next, a few straightforward controls are attempted, but one consistent observation in all cases is the difficulty of controlling the ankle angle and its effects on the crank dynamics. A "fixed-ankle" approach is adopted for physical and for analytical reasons. The challenge in controlling forward cycling for this model for the most part reduces to controlling the ankle angles through the cycle. Several approaches are examined which narrow

the range in which the ankle angle lies, including the physical limitations of the ankle angle, analysis of the terms which scale the input torques, and analysis of the effort exerted to drive the cycle using feedback linearization. The results presented illustrate the requirements to achieve forward cycling for this model.

3.2 Physical Limits of the Ankle Angle

The first consideration for the Three Degree-of-Freedom model is the physical range within which the foot can move relative to the calf. Identification of the physical range of the foot limits the scope of the analysis to that which can be achieved in reality. The foot is not free to rotate fully through an entire range of angles, but is constrained to a specific interval. The "knee-ankle-toe" angle pictured in Figure 3.1, which measures the angle between the calf and the foot, is expressed as

$$\phi = \pi - \theta_2 + \theta_3$$
$$\phi \in [\gamma_1, \gamma_2]$$

where θ_3 is the ankle angle as defined in Figure 1.1, and θ_2 is the angle of the calf relative to the horizontal. Thus, θ_3 is really the angle of the foot relative to the

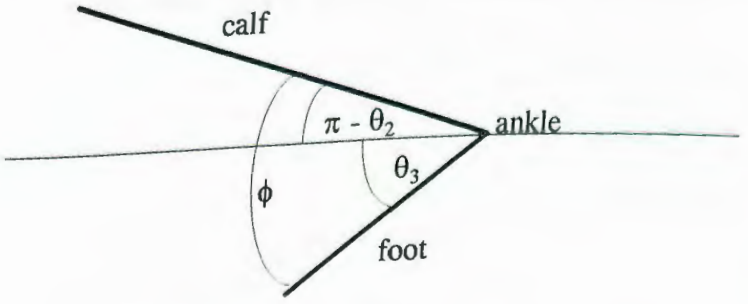

Figure 3.1: Ankle Geometry

horizontal. The expression above can be applied to either the left or right limbs, and, given a crank angle θ_4, maps the angle between the calf and the foot ϕ into the ankle angle θ_3. Thus, this expression can be used to find the range of values for θ_3 which represents the physical range of the foot. However, recall that

$$\theta_2 = f(\theta_3, \theta_4)$$

so the values of θ_3 defining the physical range cannot be found by direct solution. To define the boundaries of the physical range, we want to find the curves for θ_4 in the interval [0, 2π] such that $\phi = \gamma_1$ and $\phi = \gamma_2$. The region between these curves is the physical range of the ankle angle θ_3. The ankle angle $\theta_3(\theta_4, \gamma)$ can be computed at any θ_4 by finding solutions to the expression

$$(\phi(\theta_3, \theta_4) - \gamma)^2 = (\pi - \theta_2(\theta_3, \theta_4) + \theta_3 - \gamma)^2 = 0 \quad \gamma = \gamma_1, \gamma_2$$

Computationally, this can be found by solving the expression with θ_4 fixed and θ_3 varied until the conditions of the expression listed above are satisfied. The physical ranges of the left ankle angle for upright cycling with the parameters listed in Appendix A are shown in Figure 3.2; the solutions to the equation listed above were found using MATLAB's simplex search optimization function "fmins". The ranges for the right ankle are the same as those shown in Figure 3.2, but shifted 180°.

Figure 3.2 illustrates several important points. First, recall from Figure 1.2 that $\theta_3 > 0$ means that the foot is below the horizontal, and $\theta_3 < 0$ means that the foot is above the horizontal. Thus, from Figure 3.2, the foot is freer to move when below horizontal than above it. In fact, if the ankle is fixed throughout the cycle, then the ankle cannot remain above the horizontal. The figure also shows that in order for the foot to remain close to perpendicular to the calf (i.e. $\phi = 90°$), the ankle angle, θ_3, must be close to 90°, forcing the calf to be nearly parallel to the horizontal and the foot to be nearly vertical. The curves will change slightly as the cyclist parameters change; however, the parameters used to compute the curves in this figure are considered to be representative of an actual cyclist.

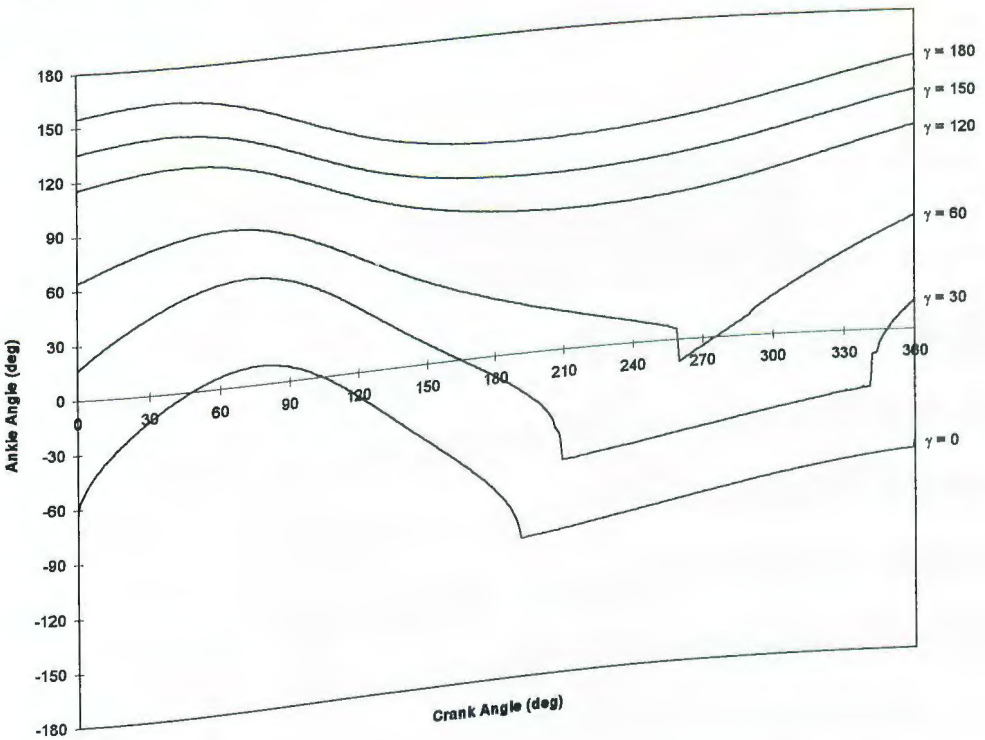

Figure 3.2: Physical Range of Ankle Angle, Upright Cycling

3.3 Reformulation of the Dynamic Equations

The dynamic equations for two-legged pedaling with the Three Degree-of-Freedom cycling model are presented in section 1.3.1 and in section 2.2 of Reference 6. The model consists of two thighs, two calves, and two ankles, with the feet attached to the cycle pedals. The format of the dynamic equations in Chapter 1 is not particularly useful for computation in that the three dynamic variables - θ_3, θ'_3, θ_4 - are included in each of the three differential equations making up the model. To facilitate analysis and simulation, separate expressions for each dynamic variable are required. The dynamics for the Three Degree-of-Freedom model two-legged pedaling can be expressed in the vector form

$$\ddot{\bar{\theta}} = \bar{f}(\bar{\theta}, \dot{\bar{\theta}}) + \bar{g}(\bar{\theta})\bar{u}$$

where

$$\bar{\theta} = \begin{bmatrix} \theta_3 \\ \theta'_3 \\ \theta_4 \end{bmatrix}, \quad \bar{f}(\bar{\theta}, \dot{\bar{\theta}}) = \begin{bmatrix} f_3(\theta_3, \dot{\theta}_3, \theta'_3, \dot{\theta}'_3, \theta_4, \theta'_4) \\ f'_3(\theta_3, \dot{\theta}_3, \theta'_3, \dot{\theta}'_3, \theta_4, \theta'_4) \\ f_4(\theta_3, \dot{\theta}_3, \theta'_3, \dot{\theta}'_3, \theta_4, \theta'_4) \end{bmatrix}$$

where $\ddot{\theta}$ is the angular acceleration, and u is the applied torque through the ankles, hips, and knees. Thus, f represents the unforced angular acceleration, and g represents the effects of the geometry on the input. Note that the f-functions are functions of both position and velocity, whereas the g-functions are functions of position only. Thus, the g-functions depend only on the cycle-cyclist geometry, and not on the full state. The complete model dynamics are expressed as

$$\ddot{\theta}_3 = f_3(\theta_3,\dot{\theta}_3,\theta_3',\dot{\theta}_3',\theta_4,\dot{\theta}_4) + g_{3_{al}}(\theta_3,\theta_3',\theta_4)u_{al} + g_{3_{ar}}(\theta_3,\theta_3',\theta_4)u_{ar} + g_{3_{hl}}(\theta_3,\theta_3',\theta_4)u_{hl}$$
$$+g_{3_{hr}}(\theta_3,\theta_3',\theta_4)u_{hr} + g_{3_{kl}}(\theta_3,\theta_3',\theta_4)u_{kl} + g_{3_{kr}}(\theta_3,\theta_3',\theta_4)u_{kr}$$
$$\ddot{\theta}_3' = f_3'(\theta_3,\dot{\theta}_3,\theta_3',\dot{\theta}_3',\theta_4,\dot{\theta}_4) + g'_{3_{al}}(\theta_3,\theta_3',\theta_4)u_{al} + g'_{3_{ar}}(\theta_3,\theta_3',\theta_4)u_{ar} + g'_{3_{hl}}(\theta_3,\theta_3',\theta_4)u_{hl}$$
$$+g'_{3_{hr}}(\theta_3,\theta_3',\theta_4)u_{hr} + g'_{3_{kl}}(\theta_3,\theta_3',\theta_4)u_{kl} + g'_{3_{kr}}(\theta_3,\theta_3',\theta_4)u_{kr}$$
$$\ddot{\theta}_4 = f_4(\theta_3,\dot{\theta}_3,\theta_3',\dot{\theta}_3',\theta_4,\dot{\theta}_4) + g_{4_{al}}(\theta_3,\theta_3',\theta_4)u_{al} + g_{4_{ar}}(\theta_3,\theta_3',\theta_4)u_{ar} + g_{4_{hl}}(\theta_3,\theta_3',\theta_4)u_{hl}$$
$$+g_{4_{hr}}(\theta_3,\theta_3',\theta_4)u_{hr} + g_{4_{kl}}(\theta_3,\theta_3',\theta_4)u_{kl} + g_{4_{kr}}(\theta_3,\theta_3',\theta_4)u_{kr}$$

where

$$f_3 = -\frac{Q_3}{h_{11}} + \frac{-h_{12}h_{21}h'_{11}Q_3 - h_{11}h_{12}h'_{21}Q_{3'} + h_{11}h_{12}\,h'_{11}Q_4 + h_{11}h_{12}h'_{11}u_D}{h_{11}(-(h_{11}h'_{12}h'_{21}) + h'_{11}(-(h_{12}h_{21}) + h_{11}(h_{22}+h'_{22})))}$$

$$f_3' = \frac{-Q_{3'}}{h'_{11}} + \frac{-h'_{11}h_{21}h'_{12}Q_3 - h_{11}h'_{12}h'_{21}Q_{3'} + h'_{11}h_{11}h'_{12}Q_4 + h'_{11}h_{11}h'_{12}u_D}{h'_{11}(-(h_{11}h'_{12}h'_{21}) + h'_{11}(-(h_{12}h_{21}) + h_{11}(h_{22}+h'_{22})))}$$

$$f_4 = \frac{h_{21}h'_{11}Q_3 + h_{11}h'_{21}Q_{3'} - h_{11}h'_{11}Q_4 - h_{11}h'_{11}u_D}{-(h_{11}h'_{12}h'_{21}) + h'_{11}(-(h_{12}h_{21}) + h_{11}(h_{22}+h'_{22}))}$$

with

$$Q_3 = h_{14}\dot{\theta}_3^2 + h_{15}\dot{\theta}_4^2 + h_{15}\dot{\theta}_3\dot{\theta}_4$$
$$Q_{3'} = h'_{13}\dot{\theta}_3^2 + h'_{14}\dot{\theta}_4^2 + h'_{15}\dot{\theta}_3'\dot{\theta}_4'$$
$$Q_4 = h_{23}\dot{\theta}_3^2 + h_{23}\dot{\theta}_3'^2 + (h_{24}+h'_{24})\dot{\theta}_4^2 + (h_{25}\dot{\theta}_3 + h'_{25}\dot{\theta}_3')\dot{\theta}_4$$

where f, Q, and h functions are functions of the crank and ankle angle positions and velocities. The g-functions are expressed as follows:

Left Ankle terms

$$g_{3_{al}}(\theta_3,\theta_3,\theta_4)=\frac{h_{19}h_{22}h'_{11}-h_{12}h_{29}h'_{11}-h_{19}h'_{12}h'_{21}+h_{19}h'_{11}h'_{22}}{-(h_{12}h_{21}h'_{11})+h_{11}h_{22}h'_{11}-h_{11}h'_{12}h'_{21}+h_{11}h'_{11}h'_{22}}$$

$$g_{3_{ar}}(\theta_3,\theta_3,\theta_4)=\frac{h_{12}(-(h'_{19}h'_{21})+h'_{11}h'_{29})}{h_{12}h_{21}h'_{11}-h_{11}h_{22}h'_{11}+h_{11}h'_{12}h'_{21}-h_{11}h'_{11}h'_{22}}$$

$$g_{3_{hl}}(\theta_3,\theta_3,\theta_4)=\frac{h_{17}h_{22}h'_{11}-h_{12}h_{27}h'_{11}-h_{17}h'_{12}h'_{21}+h_{17}h'_{11}h'_{22}}{-(h_{12}h_{21}h'_{11})+h_{11}h_{22}h'_{11}-h_{11}h'_{12}h'_{21}+h_{11}h'_{11}h'_{22}}$$

$$g_{3_{hr}}(\theta_3,\theta_3,\theta_4)=\frac{h_{12}(-(h'_{17}h'_{21})+h'_{11}h'_{27})}{h_{12}h_{21}h'_{11}-h_{11}h_{22}h'_{11}+h_{11}h'_{12}h'_{21}-h_{11}h'_{11}h'_{22}}$$

$$g_{3_{kl}}(\theta_3,\theta_3,\theta_4)=\frac{h_{19}h_{22}h'_{11}-h_{12}h_{28}h'_{11}-h_{18}h'_{12}h'_{21}+h_{18}h'_{11}h'_{22}}{-(h_{12}h_{21}h'_{11})+h_{11}h_{22}h'_{11}-h_{11}h'\,h'_{21}+h_{11}h'_{11}h'_{22}}$$

$$g_{3_{kr}}(\theta_3,\theta_3,\theta_4)=\frac{h_{12}(-(h'_{18}h'_{21})+h'_{11}h'_{28})}{h_{12}h_{21}h'_{11}-h_{11}h_{22}h'_{11}+h_{11}h'_{12}h'_{21}-h_{11}h'_{11}h'_{22}}$$

Right Ankle terms:

$$g'_{3_{al}}(\theta_3,\theta_3,\theta_4)=\frac{(h_{19}h_{21}-h_{11}h_{29})\,h'_{12}}{-(h_{12}h_{21}h'_{11})+h_{11}h_{22}h'_{11}-h_{11}h'_{12}h'_{21}+h_{11}h'_{11}h'_{22}}$$

$$g'_{3_{ar}}(\theta_3,\theta_3,\theta_4)=\frac{-(h_{12}h_{21}h'_{19})+h_{11}h_{22}h'_{19}+h_{11}h'_{19}h'_{22}-h_{11}h'_{12}h'_{29}}{-(h_{12}h_{21}h'_{11})+h_{11}h_{22}h'_{11}-h_{11}h'_{12}h'_{21}+h_{11}h'_{11}h'_{22}}$$

$$g'_{3_{hl}}(\theta_3,\theta_3,\theta_4)=\frac{(h_{17}h_{21}-h_{11}h_{27})\,h'_{12}}{-(h_{12}h_{21}h'_{11})+h_{11}h_{22}h'_{11}-h_{11}h'_{12}h'_{21}+h_{11}h'_{11}h'_{22}}$$

$$g'_{3_{hr}}(\theta_3,\theta_3,\theta_4)=\frac{-(h_{12}h_{21}h'_{17})+h_{11}h_{22}h'_{17}+h_{11}h'_{17}h'_{22}-h_{11}h'_{12}h'_{27}}{-(h_{12}h_{21}h'_{11})+h_{11}h_{22}h'_{11}-h_{11}h'_{12}h'_{21}+h_{11}h'_{11}h'_{22}}$$

$$g'_{3_{kl}}(\theta_3,\theta_3,\theta_4)=\frac{(h_{18}h_{21}-h_{11}h_{28})\,h'_{12}}{-(h_{12}h_{21}h'_{11})+h_{11}h_{22}h'_{11}-h_{11}h'_{12}h'_{21}+h_{11}h'_{11}h'_{22}}$$

$$g'_{3_{kr}}(\theta_3,\theta_3,\theta_4)=\frac{-(h_{12}h_{21}h'_{18})+h_{11}h_{22}h'_{18}+h_{11}h'_{18}h'_{22}-h_{11}h'_{12}h'_{28}}{-(h_{12}h_{21}h'_{11})+h_{11}h_{22}h'_{11}-h_{11}h'_{12}h'_{21}+h_{11}h'_{11}h'_{22}}$$

Crank angle terms

$$g_{4_{al}}(\theta_3,\theta_3,\theta_4)=\frac{(-(h_{19}h_{21})+h_{11}h_{29})h'_{11}}{-(h_{12}h_{21}h'_{11})+h_{11}h_{22}h'_{11}-h_{11}h'_{12}h'_{21}+h_{11}h'_{11}h'_{22}}$$

$$g_{4_{ar}}(\theta_3,\theta_3,\theta_4)=\frac{h_{11}(-(h'_{19}h'_{21})+h'_{11}h'_{29})}{-(h_{12}h_{21}h'_{11})+h_{11}h_{22}h'_{11}-h_{11}h'_{12}h'_{21}+h_{11}h'_{11}h'_{22}}$$

$$g_{4_{kl}}(\theta_3,\theta_3,\theta_4)=\frac{(-(h_{17}h_{21})+h_{11}h_{27})h'_{11}}{-(h_{12}h_{21}h'_{11})+h_{11}h_{22}h'_{11}-h_{11}h'_{12}h'_{21}+h_{11}h'_{11}h'_{22}}$$

$$g_{4_{kr}}(\theta_3,\theta_3,\theta_4)=\frac{h_{11}(-(h'_{17}h'_{21})+h'_{11}h'_{27})}{-(h_{12}h_{21}h'_{11})+h_{11}h_{22}h'_{11}-h_{11}h'_{12}h'_{21}+h_{11}h'_{11}h'_{22}}$$

$$g_{4_{hl}}(\theta_3,\theta_3,\theta_4)=\frac{(-(h_{18}h_{21})+h_{11}h_{28})h'_{11}}{-(h_{12}h_{21}h'_{11})+h_{11}h_{22}h'_{11}-h_{11}h'_{12}h'_{21}+h_{11}h'_{11}h'_{22}}$$

$$g_{4_{hr}}(\theta_3,\theta_3,\theta_4)=\frac{h_{11}(-(h'_{18}h'_{21})+h'_{11}h'_{28})}{-(h_{12}h_{21}h'_{11})+h_{11}h_{22}h'_{11}-h_{11}h'_{12}h'_{21}+h_{11}h'_{11}h'_{22}}$$

This reformulation of the dynamics helps to better identify the critical parts of the system and to isolate the forced and unforced parts of the dynamics. Appendix B provides MATLAB program listings illustrating how these equations were implemented for simulation.

3.4 Analysis of the g-functions

The *g*-functions are functions of the ankle and crank angles only, not of their velocities. Hence, the "weights" applied to the inputs by these functions depend only on the geometry of the system. Since these terms multiply the inputs, any combination of ankle and crank angles such that a *g*-function is zero identifies a configuration such that the input applied to that *g*-function has no effect on the associated dynamic state variable. These regions are the result of alignment of the limbs in configurations which reduce the effect of the input torque transmitted to

the joints. Thus, the ankle angle could get stuck if the velocity was near zero, or the ankle angle could become unstable if the velocity was non-negligible. Identification of these regions is important for fixing the ankle angles to prevent a loss of control and possible instability. To find points at which the g-functions were zero, the following method was used given the cyclist parameters specified in Appendix A - compute an array z_{xn} such that

$$z_{x_n}(\theta_3, \theta_4) = g_x(\theta_3, \theta_3', \theta_4)$$
$$x = 3_{al}, 3'_{ar}$$
$$\theta_3 \text{ within physical limits of Figure } 3.2$$
$$\theta_3' = \theta_3 + kn,\ k = 10,\ n = -5 \ldots +5$$
$$\theta_4 \in [0, 2\pi]$$

Thus, the left and right ankle angles were constrained to be with ± 50° of one another. For upright cycling the physical range for the ankle angles is approximately [-90°, 180°], based on Figure 3.2. Each array z was computed for a specific instance of n, so that the set of arrays for a particular g-function shows how the g-function varies from changes in the left-right ankle angle difference. Finally, MATLAB's "contour" function was used to find a locus of points in each z array where $g = 0$. Figure 3.3 shows the resulting contours for upright cycling, with "left" referring to the left ankle input term g_{3al}, and "right" referring to the right ankle input term $g_{3'ar}$. The separate contours evident in Figure 3.3 represent separate instances of n. The plot, in addition to showing that zero contours exist for the ankle g-functions, shows that the contours do not vary greatly with the difference in the left and right ankle angles. Hence, the contours are a robust

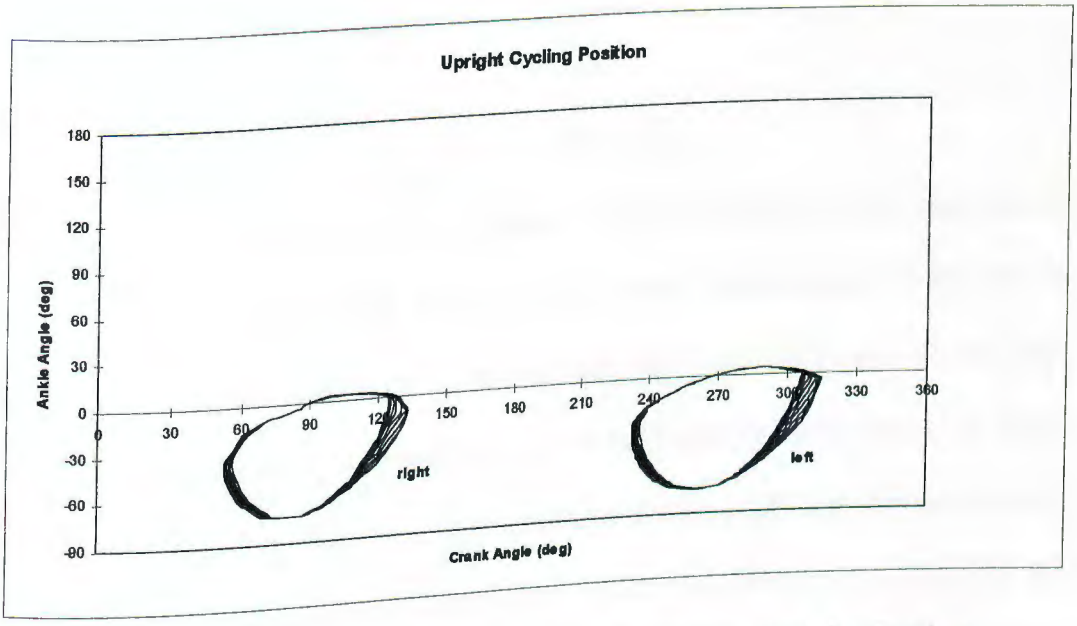

Figure 3.3: Zero Functions of Ankle *g*-functions, Upright Cycling

representation of the zero regions of the ankle *g*-functions for the ankle angles of interest. Control strategies for upright cycling for the Three Degree-of-Freedom model should ideally avoid the regions where the ankle g-function contours become zero in order to ensure control of the ankles over the entire crank cycle. From the figures, these regions are approximately

$$\theta_3, \theta_3' \in [5°, 180°]$$

3.5 Minimal Time Cycling

As with the one Degree-of-Freedom model, the goal is to find a state trajectory to minimize the cycle time cost function J over a full rotation of the crank, expressed as

$$J = \int_{t_0}^{t_f} dt$$

$$\theta_4(t_0) = \theta_4(t_f) = \theta_{4_0}$$

Unlike the One Degree-of-Freedom model, the ankle dynamics figure significantly in the dynamics of the crank angle, and complicate identification of an optimal strategy. Initial attempts at driving the cycle through bang-bang inputs in the hips, knees, and ankles were unsuccessful, due to the divergent behavior of the ankle angle. The unconstrained ankle angle tended to change position to the point where the alignment of the foot, calf, and thigh reduced the effect of the inputs at the ankle, knee, and hip. Thus, a strategy was adopted to use bang-bang input to drive the hip and knee joints and minimize the impact of the ankles by minimizing variation in θ_3 and θ'_3 through the rotation of the crank angle. Only control strategies which kept the ankle angles fixed or nearly fixed through the entire cycle were considered; i.e.

$$\left|\theta_3(t) - \hat{\theta}_3\right| < \varepsilon_3 \text{ for } t \in [t_0, t_1]$$

$$\left|\theta'_3(t) - \hat{\theta}'_3\right| < \varepsilon_{3'} \text{ for } t \in [t_0, t_1]$$

where $\hat{\theta}_3, \hat{\theta}'_3$ are the angles to which the left and right ankles are controlled, and ε_3 and $\varepsilon_{3'}$ define how tightly the ankles are controlled. This strategy is advantageous in that it can be implemented easily with strong position or velocity feedback control or a combination of position and velocity feedback of the ankle angle. Additionally, it simplifies the dynamics by keeping the ankle angular velocity $\dot{\theta}_3$ and acceleration $\ddot{\theta}_3$ close to zero. Finally, it has a basis physically - analysis of

bicycle racers [Ref. 9] has shown that over a full crank rotation, the ankle angles change relatively little compared to the hip and knee angle movements. Variation in the ankle angle in a typical racer is limited to about 10° from the mean position, which is horizontal (i.e. $\theta_3 = 0°$).

3.6 Ankle Feedback Input Strategies for Minimum Cycle Time

Next, the optimization problem presented in section 2.4.4 to learn the optimal hip and knee switchpoints is repeated. Only the third case is considered, in which two switches occurred per cycle, and the hip and knee switchpoints are optimized separately. The left and right hip and knee inputs are assumed to be opposite in polarity but synchronized with respect to switchpoints. The ankle inputs are controlled through a combination of position and velocity control. Additionally, the left and right ankles are controlled to the same fixed ankle angle. Thus,

$$u_{hip}(\theta_4) = \begin{cases} U_1 \text{ for } \theta_4 < \theta_{s_{hip1}}, \theta_4 > \theta_{s_{hip2}} \\ U_2 \text{ for } \theta_{s_{hip1}} \le \theta_4 \le \theta_{s_{hip2}} \end{cases}$$

$$u_{knee}(\theta_4) = \begin{cases} U_1 \text{ for } \theta_4 < \theta_{s_{knee1}}, \theta_4 > \theta_{s_{knee2}} \\ U_2 \text{ for } \theta_{s_{knee1}} \le \theta_4 \le \theta_{s_{knee2}} \end{cases}$$

$$u_a(\theta_3) = K_p(\hat{\theta}_3 - \theta_3) + K_v(\dot{\theta}_{3_{des}} - \dot{\theta}_3)$$

$$\hat{\theta}_3 = \hat{\theta}'_3$$

where K_p is the gain for the position feedback, and K_v is the gain for the velocity feedback.

Table 3.1: Optimal Hip and Knee Switchpoints with Ankle Feedback Control

K_{ap}	K_{av}	θ_3 control point	t_{cycle} (seconds)	θ_{sknee1}	θ_{sknee2}	θ_{ship1}	θ_{ship2}
0	100	50°	0.79	6°	77°	183°	268°
100	100	30°	0.89	33°	44°	134°	295°
500	0	50°	0.87	6°	77°	192°	268°
100	100	50°	0.88	57°	81°	193°	246°

The results for several different ankle control points and for various types of ankle feedback control are summarized in Table 3.1. Clearly, the optimal switchpoints can be "learned" for a variety of cases, but with quite different results from the one-degree of freedom model analysis. The hip switchpoints are in the vicinity of the nominal hip switchpoints for the one Degree-of-Freedom model. However, the knee switchpoints are quite different, since the ankle and the knee are connected by the calf, and changes in the ankle position greatly affect the knee angle. Thus, the optimal switchpoints for the knee and hip inputs in the One Degree-of-Freedom do not necessarily apply for the Three Degree-of-Freedom model, and the optimal switchpoints may not fall at the points at which the hip and knee angles reach extremal values. The cycle times are longer for the Three Degree-of-Freedom model cases compared to the One Degree-of-Freedom results in section 2.4 since a smaller hip and knee torque magnitude was used (see Appx. A).

Figure 3.3 shows the joints angles for the fourth case listed in Table 3.1. The combination of position and velocity feedback control on the ankle input is effective in controlling the ankle angle, and permits the crank arm to be driven by the hip and knee torques. This figure shows that forward cycling can be facilitated with a fixed-ankle strategy coupled with bang-bang inputs at the other joints.

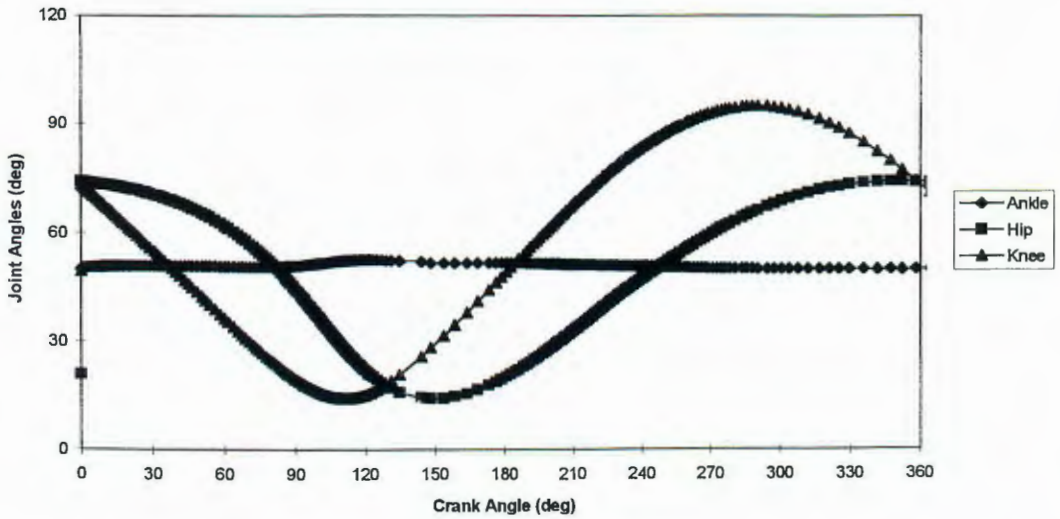

Figure 3.3: Joint Angles with Bang-Bang Hip and Knee Input, Feedback Control of Ankles

3.7 Feedback Linearization

To examine fixed ankle control further, we apply a technique known as feedback linearization which will reduce the system dynamics to a simplified linear form. Additionally, it will provide a method for computing the input signals required to achieve the linearized dynamics. Hence, the linearized dynamics can be configured to produce zero ankle velocity.

Again we express the Three Degree-of-Freedom system in a concise vector format as

$$\ddot{\bar{\theta}} = \bar{f}(\bar{\theta}, \dot{\bar{\theta}}) + \bar{g}(\bar{\theta})\bar{u}$$

where

$$\bar{\theta} = \begin{bmatrix} \theta_3 \\ \theta_3' \\ \theta_4 \end{bmatrix}, \quad \bar{f}(\bar{\theta}, \dot{\bar{\theta}}) = \begin{bmatrix} f_3(\theta_3, \dot{\theta}_3, \theta_3', \dot{\theta}_3', \theta_4, \theta_4') \\ f_3'(\theta_3, \dot{\theta}_3, \theta_3', \dot{\theta}_3', \theta_4, \theta_4') \\ f_4(\theta_3, \dot{\theta}_3, \theta_3', \dot{\theta}_3', \theta_4, \theta_4') \end{bmatrix}$$

$$g(\bar{\theta}, \dot{\bar{\theta}}) = \begin{bmatrix} g_{3_{al}}(\theta_3, \theta_3, \theta_4) & g_{3_{ar}}(\theta_3, \theta_3, \theta_4) & g_{3_{hl}}(\theta_3, \theta_3, \theta_4) & g_{3_{hr}}(\theta_3, \theta_3, \theta_4) & g_{3_{kl}}(\theta_3, \theta_3, \theta_4) & g_{3_{kr}}(\theta_3, \theta_3, \theta_4) \\ g'_{3_{al}}(\theta_3, \theta_3, \theta_4) & g'_{3_{ar}}(\theta_3, \theta_3, \theta_4) & g'_{3_{hl}}(\theta_3, \theta_3, \theta_4) & g'_{3_{hr}}(\theta_3, \theta_3, \theta_4) & g'_{3_{kl}}(\theta_3, \theta_3, \theta_4) & g'_{3_{kr}}(\theta_3, \theta_3, \theta_4) \\ g_{4_{al}}(\theta_3, \theta_3, \theta_4) & g_{4_{ar}}(\theta_3, \theta_3, \theta_4) & g_{4_{hl}}(\theta_3, \theta_3, \theta_4) & g_{4_{hr}}(\theta_3, \theta_3, \theta_4) & g_{4_{kl}}(\theta_3, \theta_3, \theta_4) & g_{4_{kr}}(\theta_3, \theta_3, \theta_4) \end{bmatrix}$$

$$\bar{u} = \begin{bmatrix} u_{al} & u_{ar} & u_{hl} & u_{hr} & u_{kl} & u_{kr} \end{bmatrix}^T$$

The feedback linearization input is defined as follows:

$$\bar{u} = \left(-\bar{g}^*(\bar{\theta})\right)\left[\bar{f}(\bar{\theta}, \dot{\bar{\theta}}) - \bar{v}\right]$$

where

$$\bar{g}(\bar{\theta})\bar{g}^*(\bar{\theta}) = I$$

Applying this input strategy to the dynamics, we find

$$\begin{aligned} \ddot{\bar{\theta}} &= \bar{f}(\bar{\theta}, \dot{\bar{\theta}}) + \bar{g}(\bar{\theta})\left(-\bar{g}^*(\bar{\theta})\right)\left[\bar{f}(\bar{\theta}, \dot{\bar{\theta}}) - \bar{v}\right] \\ &= \bar{f}(\bar{\theta}, \dot{\bar{\theta}}) - \bar{f}(\bar{\theta}, \dot{\bar{\theta}}) + \bar{v} \\ &= \bar{v} \end{aligned}$$

Thus, if we pick $\bar{v}$ as follows

$$\bar{v} = \begin{bmatrix} K_{3_p}\theta_3 + K_{3_v}\dot{\theta}_3 + K_{3_c} \\ K_{3'_p}\theta_3' + K_{3'_v}\dot{\theta}_3' + K_{3'_c} \\ K_{4_p}\theta_4 + K_{4_v}\dot{\theta}_4 + K_{4_c} \end{bmatrix}$$

then the characteristic equations of the system are

$$\text{Left Ankle:} \quad \lambda_3^2 - K_{3_v}\lambda_3 + K_{3_p}$$
$$\text{Right Ankle:} \quad \lambda_{3'}^2 - K_{3'_v}\lambda_{3'} + K_{3'_p}$$
$$\text{Crank Angle:} \quad \lambda_4^2 - K_{4_v}\lambda_4 + K_{4_p}$$

Now, to lock the ankle angles at a specific value through the entire cycle, we set the gains such that

$$\overline{v} = \begin{bmatrix} 0 \\ 0 \\ K_{4_c} \end{bmatrix}$$

which will enable the crank to accelerate at a constant rate while controlling the ankle angles to their starting positions by zeroing their acceleration. With K_{4c} set to a constant value, the time required to complete exactly one full cycle remains constant no matter what the ankle angle is. Figures 3.4 and 3.5 show sample input torque profiles for $\theta_3 = 30°$. The figures show a larger torque required at the top of the cycle (TDC; see Appendix A) than at the bottom of the cycle (BDC). Therefore, the limbs must exert more effort to push a foot through the top of the cycle, but can essentially coast through the bottom of the cycle. This indicates a possible unfavorable limb alignment at TDC.

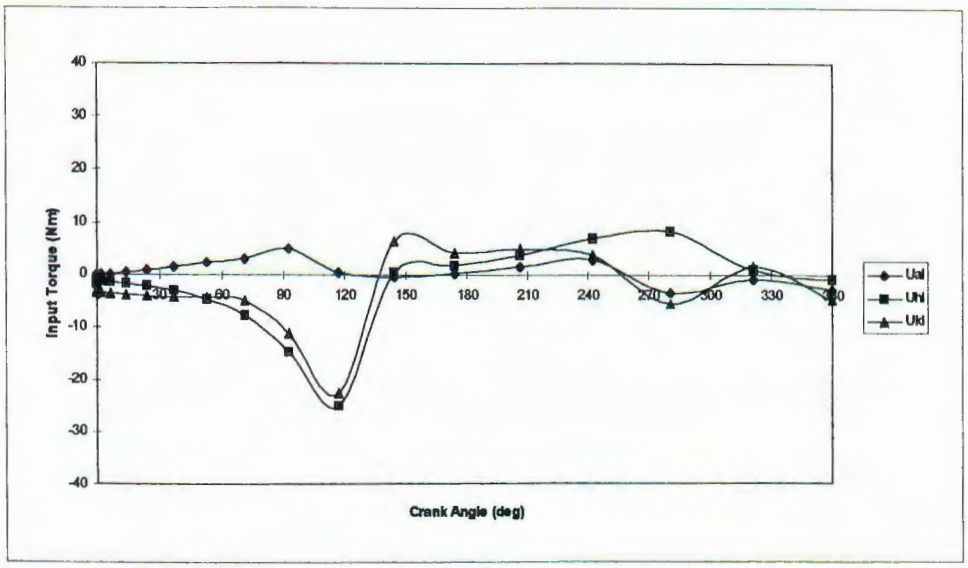

Figure 3.4: Left Limb Input Torques for Feedback Linearization with Ankles fixed at 30 degrees

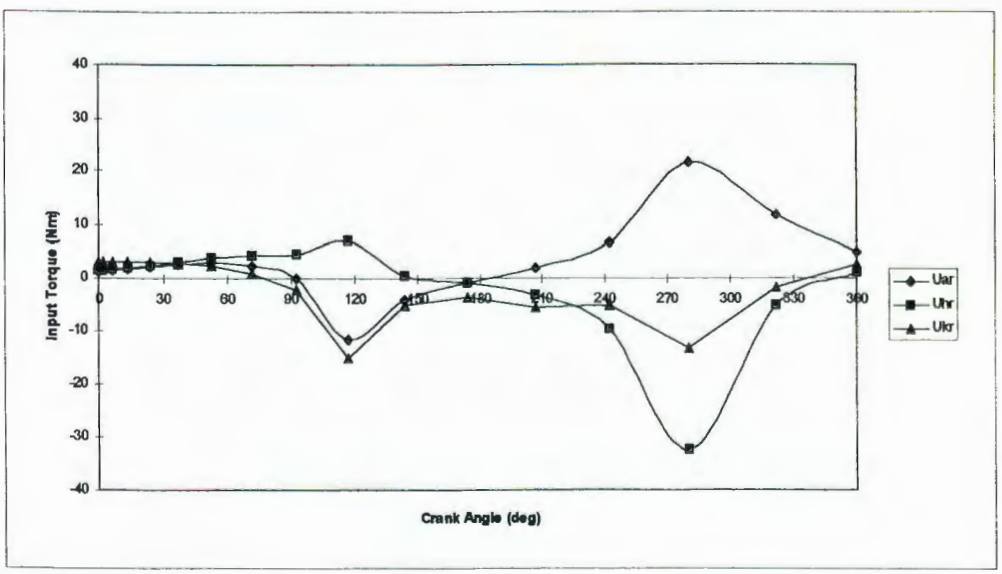

Figure 3.5: Right Limb Input Torques for Feedback Linearization with Ankles fixed at 30 degrees

3.7.1 Rank Analysis for Feedback Linearization

To successfully implement the fixed ankle strategy for feedback linearization, we need to verify that $\mathbf{rank}\left(g(\bar{\theta})\right) = 3$ for all hip and crank angle combinations in use, since $\bar{g}(\bar{\theta})$ is 3x6. If the rank is less than 3 at any point, then the feedback linearization strategy is not realizable for that combination of angles. To measure rank computationally, the Singular Value Decomposition is used. The Singular Value Decomposition Theorem (Ref. [10]) states that every *m*x*n* matrix H of rank r can be transformed into the form

$$H = U\begin{bmatrix}\Sigma & 0\\ 0 & 0\end{bmatrix}V',\ \Sigma = \mathbf{diag}\{\sigma_1, \sigma_2, ..., \sigma_r\},\ \sigma_1 \geq \sigma_2 \geq ... \geq \sigma_r > 0$$

with

$$U'U = UU' = I_m,\ V'V = VV' = I_n$$

Thus, if $\mathbf{rank}\left(g(\bar{\theta})\right) < 3$, then $\sigma_3 = 0$. Identification of combinations of $(\theta_3, \theta_3', \theta_4)$ such that $\sigma_3 = 0$ will pinpoint regions in which the alignment of the cyclist and bicycle geometry compromises the cyclist's ability to drive the crank.

One difficulty with this particular problem is that $\bar{g}(\bar{\theta})$ is a function of three variables. We obviously want to compute $\bar{g}(\bar{\theta})$ for $\forall \theta_4 \in [0, 2\pi]$, but we only need to look at θ_3 and θ'_3 over the physical range. Figure 3.6 shows pairs of left and right ankle angles against the crank angle such that $\sigma_3 \approx 0$. Computationally, the points displayed in the figure have $\sigma_3 < 10^{-6}$, and were found by using the MATLAB multivariable simplex-search optimization function "fmins" to minimize

σ_3 over $(\theta_3, \theta_3', \theta_4)$ for various starting angles incremented over the physically realizable space of $(\theta_3, \theta_3', \theta_4)$. The symbols for the left and right ankle angles in the plot represent pairs of ankle angles for a particular crank angle. The purpose of the plot is not to identify every point of rank deficiency, but to illustrate that rank deficiency occurs in distinct regions and in distinct angle combinations for upright cycling. Several aspects of Figure 3.6 are notable. First, rank deficiency occurs for $\theta_4 \approx 90^\circ$ and for $\theta_4 \approx 270^\circ$; i.e. when one foot is near TDC. In these regions, the position of the opposite ankle is largely irrelevant, as illustrated by its nearly random distribution of rank-deficient points in contrast to the well-defined contour of the foot near TDC. At this position, the foot is nearly aligned with the crank arm, as illustrated in Figure 3.7, which shows the left leg geometry with the left foot near TDC. The joints are labeled according to the convention in Figure 1.2. As the figure shows, the foot is nearly in alignment with the crank arm. In this situation, rotation of the knee will have little effect, since the tangent to the calf is close to collinear with the foot and crank arm. Hence, even a large torque exerted at the left knee will have little effect here. Figure 3.6 provides further confirmation of an unfavorable limb alignment when one foot is near the top of the cycle, as seen in Figures 3.4 and 3.5.

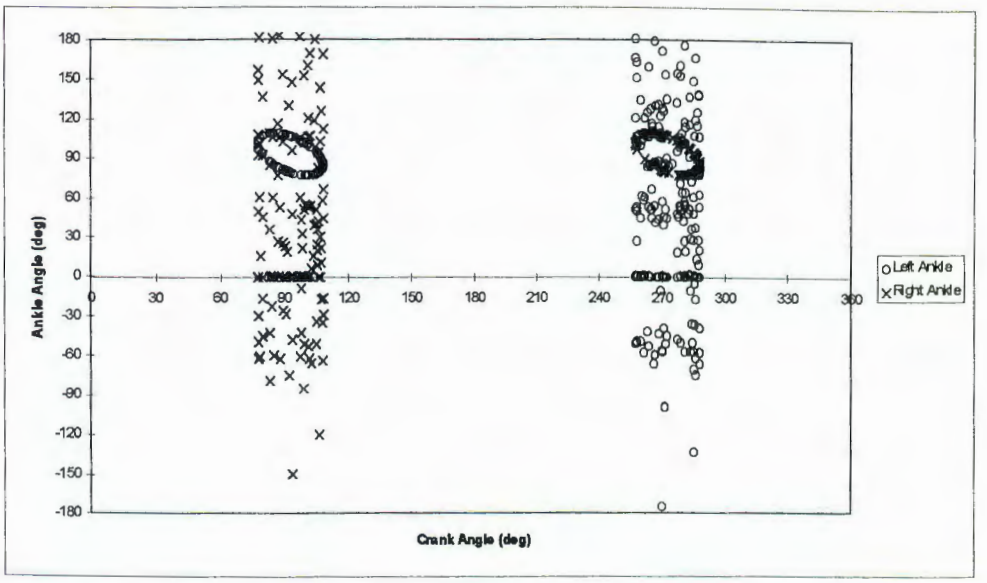

Figure 3.6: Angle Combinations Causing Rank(g) < 3

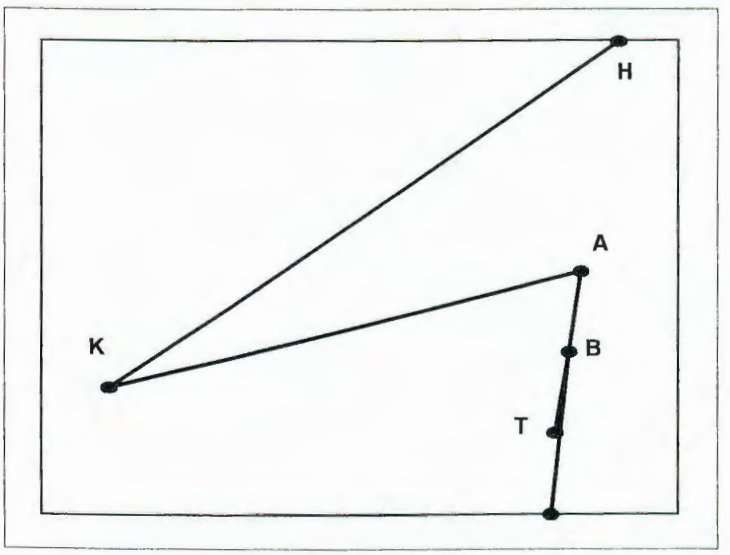

Figure 3.7: Left Leg Geometry at Subrank Condition

3.7.2 Optimization of Ankle Angle

Given the fixed ankle strategy for feedback linearization, we can find a more desirable ankle angle by computing the overall effort required to drive the cycle as

$$\int_{t_0}^{t_1} u^2 dt = \int_{t_0}^{t_1} (u_{al}^2 + u_{ar}^2 + u_{hl}^2 + u_{hr}^2 + u_{kl}^2 + u_{kr}^2) dt$$
$$\theta_4(t_1) = \theta_4(t_0) + 2\pi$$

for various ankle angles. Figure 3.8 shows the results over the full physical range of the ankle angle, with the left and right ankles controlled to the same angle, and with K_{4c} chosen as 10 to achieve a full rotation of the crank in a realistic time of 1.2 seconds. Figure 3.8 clearly shows that certain ankle angles will achieve full rotation of the crank at a lower cost in input effort; in this case, the ideal ankle angle would be about 10° for upright cycling. This is consistent with the analysis of professional cycling racers in Reference 9 showing that the foot remains nearly

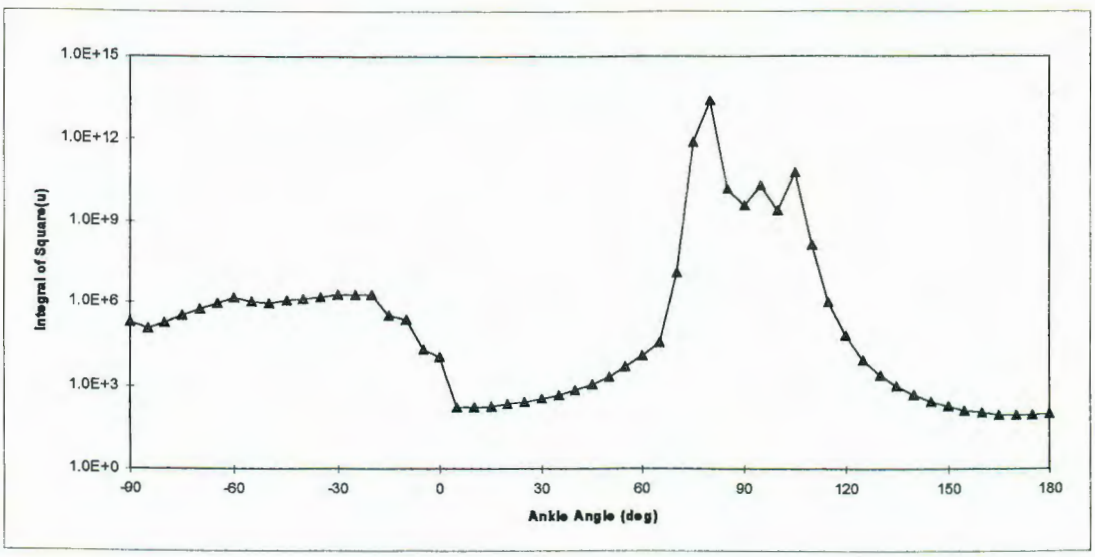

Figure 3.8: Input Effort to Complete a Full Cycle vs. Fixed Ankle Angle

horizontal through the full cycle and varies little from the mean position. The figure also shows a significantly larger effort required in the region $\theta_3 \in [75^\circ, 105^\circ]$, which is where rank deficiency in the g-matrix is evident in Figure 3.6. Recall that the g-functions are functions only of the geometry, not of the full state, so the large effort shown in Figure 3.8 in the region $\theta_3 \in [75^\circ, 105^\circ]$ is a result of singularities in the g-matrix caused by the limb geometry. It is clear to see that unfavorable limb alignments cause rank deficiency in the feedback linearization g-matrix, sharply reducing the effect of the input torques and thereby requiring a much larger effort to pedal through that geometry. Thus, we have shown that joint angle geometries which will cause the cyclist difficulty can be identified through rank analysis of the feedback linearization g-matrix, which can be accomplished simply through substitution of cyclist parameters into the Three Degree-of-Freedom model followed by computational analysis of the g-matrix in section 3.7.

3.8 Variation of Seat Height

Analysis of the results in sections 3.4 and 3.7 clearly demonstrated the difficulties in performing pedaling with the Three Degree-of-Freedom model using the Appendix A cyclist parameters. One method of possibly reducing or eliminating limb alignment problems is adjustment of the seat height. The distance from the crank center to the seat, d, is pictured in Figure 1.2. From Appendix A, the original seat height used for analysis in this chapter was d=0.6m. To examine

the effects of changing the seat height, d was changed from 0.6m to 0.8m. The seat was raised rather than lowered, since lowering the seat would merely push the thigh and calf closer together through the cycle, exacerbating rather than reducing the problem. A greater knee angle would avoid the alignment problem pictured in Figure 3.7.

With d changed to 0.8m, the physical range computations of section 3.2 were repeated, the physical range of the left ankle is shown in Figure 3.9. The limits of the physical range are similar to those in Figure 3.2; however, note that the range with the seat raised is wider near TDC, indicating greater freedom for foot movement there. Next, the g-function analysis computations of section 3.4 were repeated. With the seat raised to 0.8m, no zero contours of the ankle g-functions were found within the physical range of the foot. For all ankle angles and crank angles conforming to the conditions listed in section 3.4, it was found that

$$z_{3_{al}}(\theta_3, \theta_3', \theta_4) > 0$$
$$z_{3'_{ar}}(\theta_3, \theta_3', \theta_4) > 0$$

Thus, the left ankle input term g_{3al} and the right ankle input term $g_{3'ar}$ never cause loss of control of the ankle angle by becoming zero. Additionally, since these terms are always positive, the effect of the input torques on the model dynamics is always in the same direction as the input torques - i.e. the g-functions do not negatively multiply the input torques and reverse their effect. Hence, there are no ankle angle regions to avoid in order to maintain control, as there are with the lower seat position. Finally, the effort required to drive the crank through a full

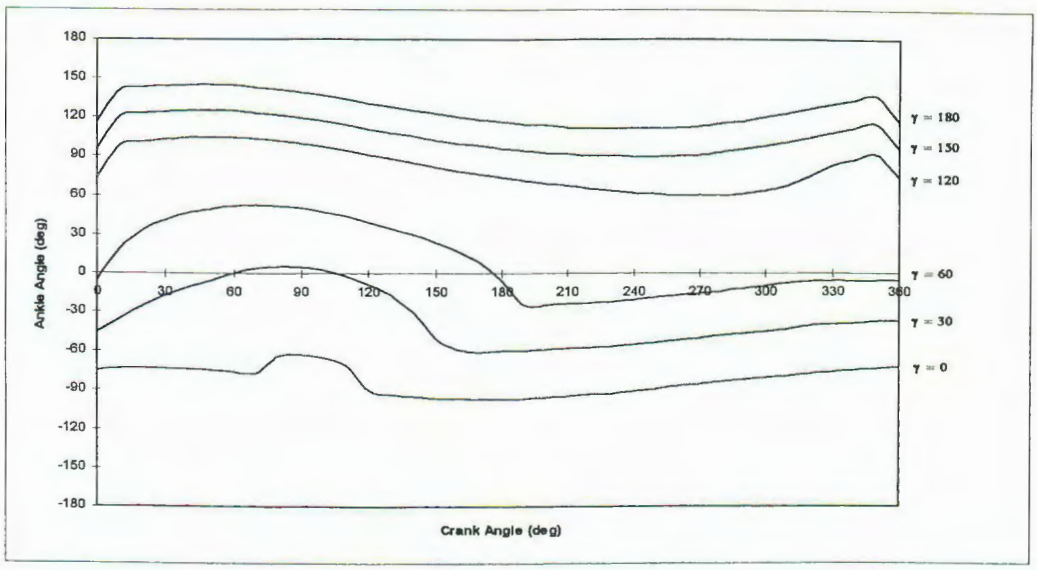

Figure 3.9: Physical Range of Ankle Angle with Raised Seat, Upright Cycling

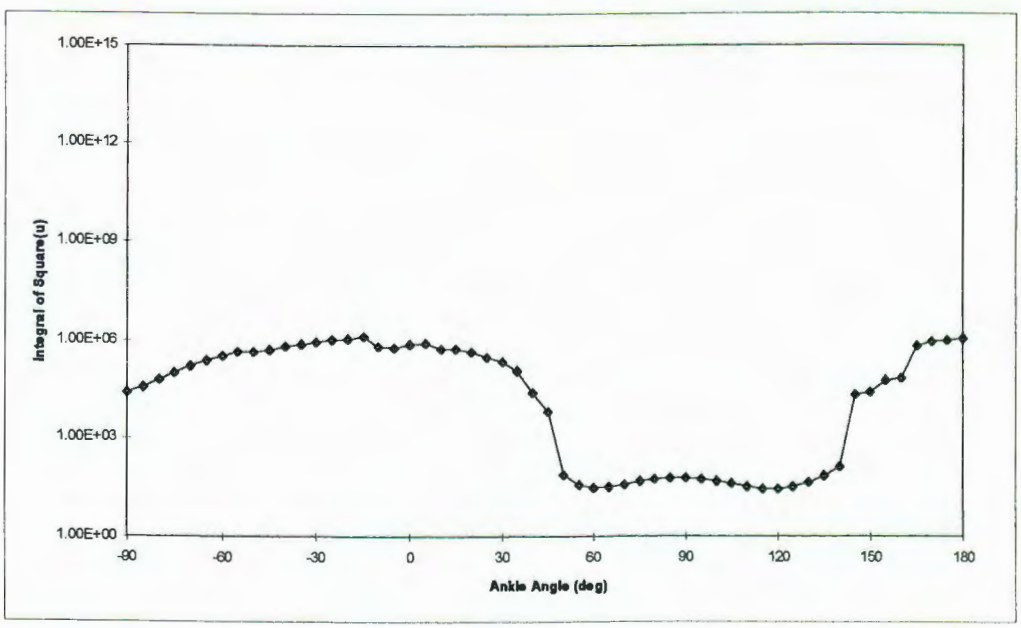

Figure 3.10: Input Effort Required to Complete a Full Cycle vs. Fixed Ankle Angle for Raised Seat

rotation was computed for the range of realistic ankle angles using feedback linearization as described in section 3.7.2, and the result is shown in Figure 3.10. The acceleration constant K_{4c} was set to 10, as it was in section 3.7.2, so the results of figures 3.8 and 3.10 can be directly compared. The effort required to pedal the cycle with the seat raised is similar to the previous case in Figure 3.8 in the regions $\theta_3 \in [-90^\circ, 0^\circ], [120^\circ, 180^\circ]$, but is significantly lower in the region $\theta_3 \in [0^\circ, 120^\circ]$, where g-matrix rank deficiency occurred with a lower seat height. Hence, the data show that raising the seat reduces or eliminates alignment problems, and allows a greater percentage of the input joint torques to be transmitted to the crank arm. It is interesting to note that experimental data in Reference 8 showing that greater power output can be obtained by raising the seat.

Choosing d=0.8m for the seat height, given the default parameter set outlined in Appendix A, probably extended the seat too high to be realistic. In comparison of Figure 3.8 and 3.10, the optimal ankle angle changed from approximately 10° with d=0.6m to approximately 60° with d=0.8, which is not a reasonable fixed ankle position, given the research presented in Reference 9 regarding actual bicycling racers. The ideal seat height would be just high enough to avoid the g-matrix singularity exhibited in Figure 3.8, but not so high as to require the foot to be significantly below the horizontal. For the parameter set used in this analysis, an acceptable seat height would be in the range of 0.7m to 0.75m.

3.9 Conclusions

In this chapter, the problem of controlling the Three Degree-of-Freedom model in forward cycling has been examined. In determining the physical range of motion for the foot, it was shown that the foot is generally freer to move below the horizontal for upright cycling, and that the range of motion is not the same for all possible crank angles. Next, the dynamic equations of the Three Degree-of-Freedom model were analyzed in detail, and areas where loss of ankle control could occur were identified. It was shown that position and velocity feedback control implemented with the goal of holding the ankle angle fixed facilitated rotation of the crank arm with bang-bang inputs at the hips and knees, and that the hip and knee bang-bang switchpoints could be optimized as they were in Chapter 2 for minimal time cycling. Finally, feedback linearization can be used to "reverse engineer" the dynamics and compute the inputs required to achieve the desired dynamics; in this analysis, constant acceleration of the crank. Perhaps most significantly, subrank conditions in the g matrix were identified and shown to be the result of unfavorable limb alignments, which when encountered, require greater effort to drive the cycle. The rank analysis and effort analysis demonstrated a method for mathematically identifying unfavorable cyclist geometries in the Three Degree-of-Freedom model. Finally, variation of the seat height was presented as a possible method for reducing or eliminating unfavorable limb alignments.

Chapter 4 Results for Three Degree-of-Freedom Recumbent Cycling

4.1 Introduction

In this chapter, the Three Degree-of-Freedom model utilized in Chapter 3 to analyze upright cycling is used to examine similar aspects of recumbent cycling. A recumbent cyclist sits behind the crank rather than sitting above it. Appendix A provides the parameter sets used to configure the model for upright and recumbent cycling. In this chapter, the physical limits on the range of the foot are presented, the behavior of the g-functions is analyzed, and weak rank points are identified, and the effort required to pedal over one cycle is presented to identify the optimal ankle angles for pedaling in a recumbent position. A seat-crank distance $d = 0.6$m was used throughout the analyses in this chapter.

4.2 Physical Limits for the Ankle Angle

As with upright cycling, the first consideration is the physical range within which the foot can move relative to the calf. Identification of the physical range of the foot limits the scope of the analysis to that which can be achieved physically. In reality, the foot is not free to move through an entire range of angles, but is constrained to a specific interval. For recumbent cycling, we would intuitively expect that the foot would on average be above the horizontal. The "knee-ankle-

toe" angle pictured in Figure 3.1, which measures the angle between the calf and the foot, is expressed as

$$\phi = \pi - \theta_2 + \theta_3$$
$$\phi \in [\gamma_1, \gamma_2]$$

where θ_3 is the ankle angle as defined in Figure 2 of Chapter 1, and θ_2 is the angle of the calf relative to the horizontal. The expression above can be applied to either the left or right limbs, and, given a crank angle θ_4, maps the angle between the calf and the foot ϕ into the ankle angle θ_3. Thus, this expression can be used to find the range of values for θ_3 which represents the physical range of the foot. To define the boundaries of the physical range, we want to find the curves for θ_4 in the interval [0, 2π] such that $\phi = \gamma_1$ and $\phi = \gamma_2$. The region between these curves is the physical range of θ_3. Repeating the method from section 3.2, the curves of $\theta_3(\theta_4, \gamma)$ can be computed by finding solutions to the expression

$$(\phi(\theta_3, \theta_4) - \gamma)^2 = (\pi - \theta_2(\theta_3, \theta_4) + \theta_3 - \gamma)^2 = 0 \quad \gamma = \gamma_1, \gamma_2$$

for incremental values of the crank angle θ_4. Computationally, this can be found by solving the expression with θ_4 fixed and θ_3 varied until the conditions of the expression listed above are satisfied.

The physical ranges of the ankle angle for recumbent cycling with the parameters listed in Appendix A are shown in Figure 4.1. This figure illustrates several points. First, the ankle angle for the most part is zero or less than zero, indicating that the foot is above the horizontal, as hypothesized. Next, the physical

range for recumbent cycling is similar to the physical range for upright cycling in that there are clear regions where the range is smaller, indicating that the rotation of the foot about the ankle has a larger effect on the calf angle, and regions where the range is larger, indicating that movement of the foot about the ankle has a smaller effect on the calf angle. For upright cycling (Figure 3.2), the smallest range is near the top of the cycle, and the largest range is near the bottom of the cycle. For recumbent cycling, the smallest range is near zero, and the largest range is near 180°.

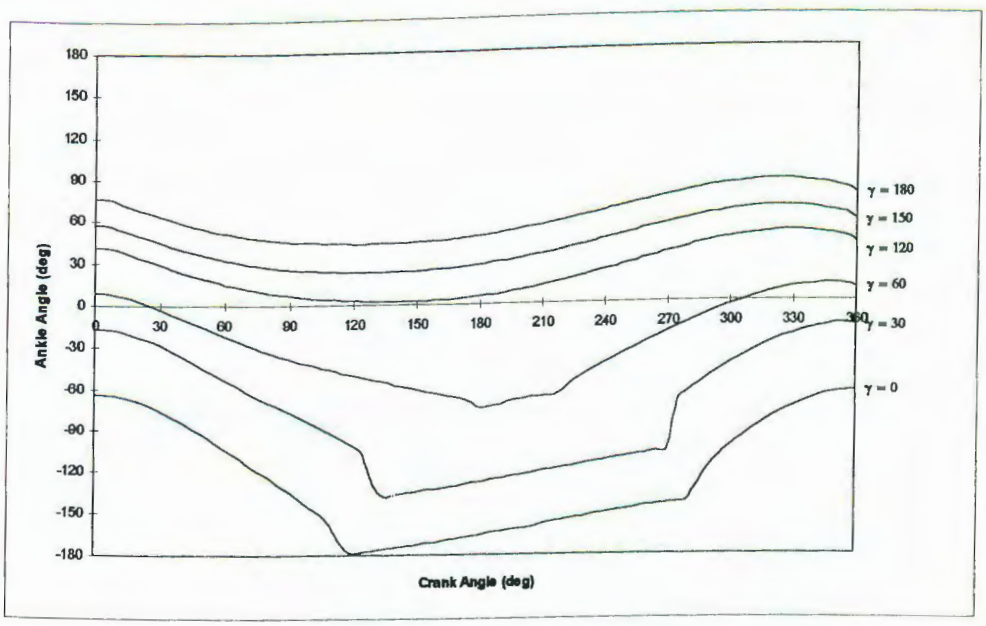

Figure 4.1: Physical Range of Ankle Angle, Recumbent Cycling

4.3 Analysis of the g-functions

The *g*-function analysis of Chapter 3 identifies joint angles at which control at the ankle joint is reduced. Since these terms multiply the inputs, any

combination of ankle and crank angles such that a g-function is zero identifies a configuration such that the input applied to that g-function has no effect on the associated dynamic state variable. These regions are the result of alignment of the limbs in configurations which reduce the effect of the input torque transmitted to the joints. Identification of these regions is important for fixing the ankle angles to prevent a loss of control and possible instability. To find points at which the g-functions were zero for recumbent cycling, the following method was used given the cyclist parameters specified in Appendix A: compute a matrix z_{xn} such that

$$z_{x_n}(\theta_3, \theta_4) = g_x(\theta_3, \theta_3', \theta_4)$$
$$x = 3_{al}, 3'_{ar}$$
$$\theta_3 \text{ within physical limits of Figure 4.1}$$
$$\theta_3' = \theta_3 + kn,\ k = 10,\ n = -5 \ldots +5$$
$$\theta_4 \in [0, 2\pi]$$

Thus, the left and right ankle angles were constrained to be close to one another. For a recumbent cycling position the physical range for the ankle angles is approximately [-180°, 90°]. Each array z_{xn} was computed for a specific instance of n, so that the set of arrays for a particular g-function shows how the g-function varies from changes in the left-right ankle angle difference. Finally, MATLAB's "contour" function was used to find a locus of points in each z_{xn} array where g = 0. Unlike the upright cycling case in Chapter 3 with the seat height at 0.6m, no zero contours were found within the physical range of the foot for recumbent cycling. For all ankle angles and crank angles conforming to the conditions listed above, it was found that

$$z_{3_{al}}(\theta_3, \theta_3', \theta_4) > 0$$
$$z_{3'_{ar}}(\theta_3, \theta_3', \theta_4) > 0$$

Thus, the left ankle input term g_{3al} and the right ankle input term $g_{3'ar}$ never cause loss of control of the ankle angle by becoming zero. Additionally, since these terms are always positive, the effect of the input torques on the model dynamics is always in the same direction as the input torques - i.e. the g-functions do not negatively multiply the input torques and reverse their effect. Hence, there are no ankle angle regions to avoid in order to maintain control, as there are for upright cycling with the seat height at 0.6m.

4.4 Feedback Linearization

As with the upright cycling model, feedback linearization can be applied to provide a method for computing the input signals required to achieve the linearized dynamics. Again we express the Three Degree-of-Freedom system in a concise vector format as

$$\ddot{\bar{\theta}} = \bar{f}(\bar{\theta}, \dot{\bar{\theta}}) + \bar{g}(\bar{\theta})\bar{u}$$

where

$$\bar{\theta} = \begin{bmatrix} \theta_3 \\ \theta_3' \\ \theta_4 \end{bmatrix}, \quad \bar{f}(\bar{\theta}, \dot{\bar{\theta}}) = \begin{bmatrix} f_3(\theta_3, \dot{\theta}_3, \theta_3', \dot{\theta}_3', \theta_4, \theta_4') \\ f_3'(\theta_3, \dot{\theta}_3, \theta_3', \dot{\theta}_3', \theta_4, \theta_4') \\ f_4(\theta_3, \dot{\theta}_3, \theta_3', \dot{\theta}_3', \theta_4, \theta_4') \end{bmatrix}$$

$$g(\bar{\theta}, \dot{\bar{\theta}}) = \begin{bmatrix} g_{3_{al}}(\theta_3, \theta_3', \theta_4) & g_{3_{ar}}(\theta_3, \theta_3', \theta_4) & g_{3_{bl}}(\theta_3, \theta_3', \theta_4) & g_{3_{br}}(\theta_3, \theta_3', \theta_4) & g_{3_{hl}}(\theta_3, \theta_3', \theta_4) & g_{3_{hr}}(\theta_3, \theta_3', \theta_4) \\ g'_{3_{al}}(\theta_3, \theta_3', \theta_4) & g'_{3_{ar}}(\theta_3, \theta_3', \theta_4) & g'_{3_{bl}}(\theta_3, \theta_3', \theta_4) & g'_{3_{br}}(\theta_3, \theta_3', \theta_4) & g'_{3_{hl}}(\theta_3, \theta_3', \theta_4) & g'_{3_{hr}}(\theta_3, \theta_3', \theta_4) \\ g_{4_{al}}(\theta_3, \theta_3', \theta_4) & g_{4_{ar}}(\theta_3, \theta_3', \theta_4) & g_{4_{bl}}(\theta_3, \theta_3', \theta_4) & g_{4_{br}}(\theta_3, \theta_3', \theta_4) & g_{4_{hl}}(\theta_3, \theta_3', \theta_4) & g_{4_{hr}}(\theta_3, \theta_3', \theta_4) \end{bmatrix}$$

$$\bar{u} = \begin{bmatrix} u_{al} & u_{ar} & u_{hl} & u_{hr} & u_{kl} & u_{kr} \end{bmatrix}^T$$

The feedback linearization input is the following:

$$\bar{u} = \left(-\bar{g}^*(\bar{\theta})\right)\left[\bar{f}(\bar{\theta}, \dot{\bar{\theta}}) - \bar{v}\right]$$

where

$$\bar{g}(\bar{\theta})\bar{g}^*(\bar{\theta}) = I$$

Applying this input strategy to the dynamics, we find

$$\begin{aligned} \ddot{\bar{\theta}} &= \bar{f}(\bar{\theta}, \dot{\bar{\theta}}) + \bar{g}(\bar{\theta})\left(-\bar{g}^*(\bar{\theta})\right)\left[\bar{f}(\bar{\theta}, \dot{\bar{\theta}}) - \bar{v}\right] \\ &= \bar{f}(\bar{\theta}, \dot{\bar{\theta}}) - \bar{f}(\bar{\theta}, \dot{\bar{\theta}}) + \bar{v} \\ &= \bar{v} \end{aligned}$$

Thus, if we pick $\bar{v}$ as follows

$$\bar{v} = \begin{bmatrix} K_{3_p}\theta_3 + K_{3_v}\dot{\theta}_3 + K_{3_c} \\ K_{3'_p}\theta'_3 + K_{3'_v}\dot{\theta}'_3 + K_{3'_c} \\ K_{4_p}\theta_4 + K_{4_v}\dot{\theta}_4 + K_{4_c} \end{bmatrix}$$

then the characteristic equations of the system are

Left Ankle: $\lambda_3^2 - K_{3_v}\lambda_3 + K_{3_p}$

Right Ankle: $\lambda_{3'}^2 - K_{3'_v}\lambda_{3'} + K_{3'_p}$

Crank Ankle: $\lambda_4^2 - K_{4_v}\lambda_4 + K_{4_p}$

Now, let us assume that our strategy is to lock the ankle angles at a specific point through the entire cycle, and drive the crank with the hip and knee inputs. Using feedback linearization, we set the gains such that

$$\overline{v} = \begin{bmatrix} 0 \\ 0 \\ K_{4_c} \end{bmatrix}$$

which will enable the crank to accelerate at a constant rate while controlling the ankle angles to their starting positions by zeroing their acceleration. With K_{4c} set to a constant, the time to complete one full cycle starting from zero remains constant no matter where the ankle angle is fixed. Figures 4.2 and 4.3 show sample input torque profiles for $\theta_3 = 30°$. The figures show that the torque required to drive the crank through a full cycle is less than that required for upright cycling (Figs. 3.8, 3.10). For recumbent cycling, a larger torque is required at the beginning of the cycle (approximately $\theta_4 = 0°$) and near the midpoint of the cycle (approximately $\theta_4 = 180°$), indicating that the limb alignment in these regions is

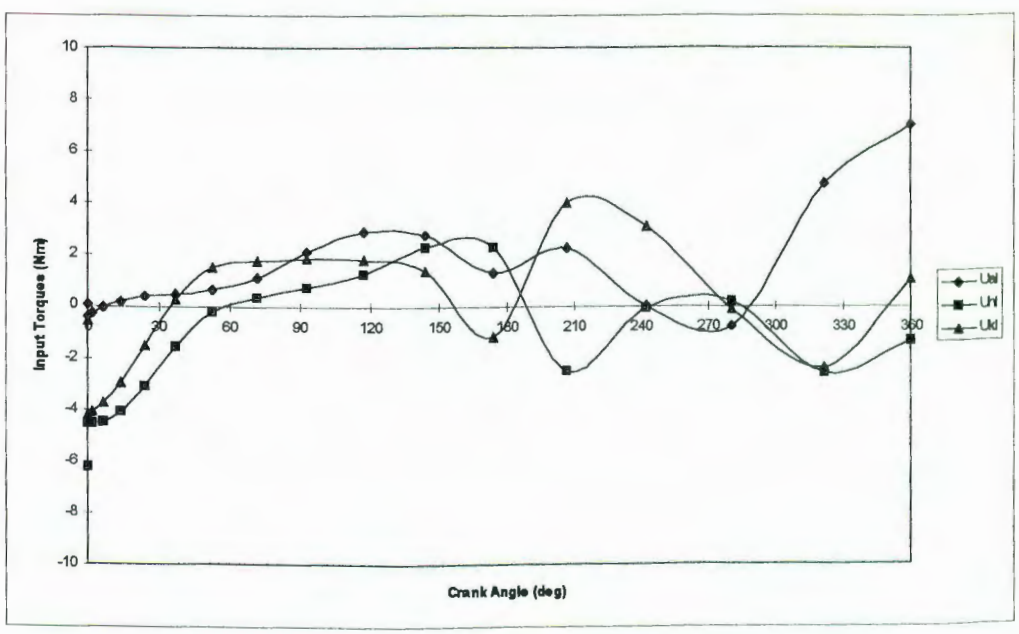

Figure 4.2: Left Limb Input Torques for Feedback Linearization with Ankles fixed at 30 degrees

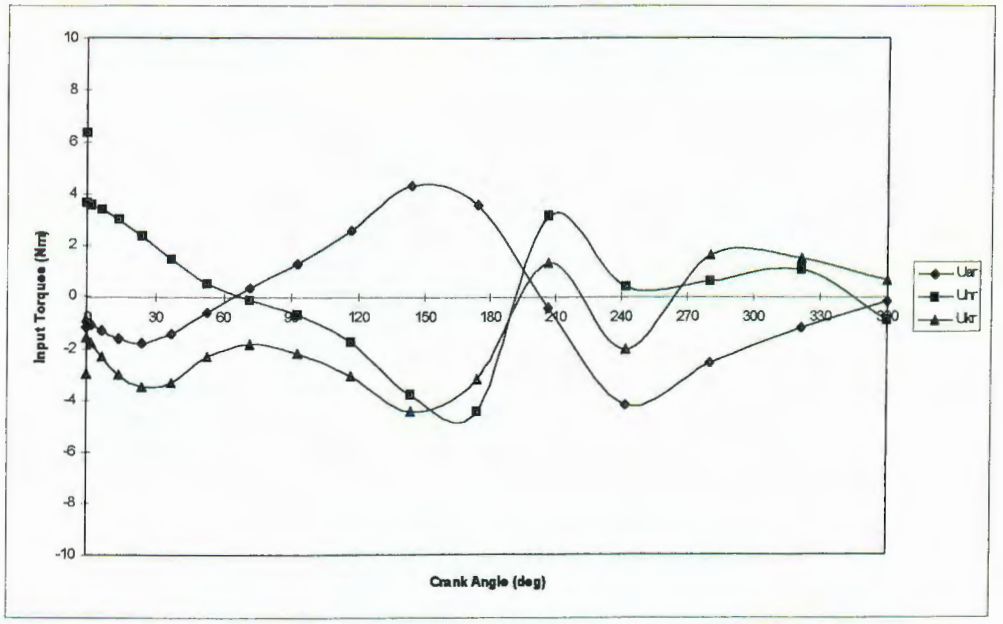

Figure 4.3: Right Limb Input Torques for Feedback Linearization with Ankles fixed at 30 degrees

slightly less favorable than in other regions.

4.4.1 Rank Analysis for Feedback Linearization

To successfully implement the fixed-ankle strategy, we need to verify that $\text{rank}\left(g(\overline{\theta})\right) = 3$ for all hip and crank angle combinations in use, since $\overline{g}(\overline{\theta})$ is 3x6. If the rank is less than 3 at any point, then the feedback linearization strategy is not realizable for that combination of angles. To measure rank computationally, the Singular Value Decomposition is used. The Singular Value Decomposition Theorem (Ref. [10]) states that every *mxn* matrix *H* of rank *r* can be transformed into the form

$$H = U\begin{bmatrix}\Sigma & 0\\ 0 & 0\end{bmatrix}V',\ \Sigma = \mathrm{diag}\{\sigma_1,\sigma_2,...,\sigma_r\},\ \sigma_1 \geq \sigma_2 \geq ... \geq \sigma_r > 0$$

with

$$U'U = UU' = I_m,\ V'V = VV' = I_n$$

One difficulty with this particular problem is that $\bar{g}(\bar{\theta})$ is a function of three variables. We obviously want to compute $\bar{g}(\bar{\theta})$ for $\theta_4 \in [0, 2\pi]$, but we only need to look at θ_3 and θ'_3 over the physical range. Figure 4.4 shows pairs of left and right ankle angles against the crank angle such that $\sigma_3 \approx 0$. Computationally, the points displayed in the figure have $\sigma_3 < 10^{-6}$, and were found by using the MATLAB multivariable simplex-search optimization function "fmins" to minimize σ_3 over $(\theta_3, \theta'_3, \theta_4)$ for various starting angles incremented over the physically realizable space of $(\theta_3, \theta'_3, \theta_4)$. The symbols for the left and right ankle angles in the plot represent pairs of ankle angles for a particular crank angle. What is notable from the plot is that no rank deficiency occurs within the physical range of the ankle angle. The only rank deficient regions are near $\theta_4 \approx 130^\circ, \theta_3 \approx -220^\circ$ and $\theta_4 \approx 305^\circ, \theta'_3 \approx -220^\circ$, but the ankle angles lie outside the physical range of the ankle angle as pictured in Figure 4.1. Hence, regions of unfavorable alignment of the limbs are not encountered as often for the recumbent cycling parameters as for the upright cycling parameters with the seat height at 0.6m.

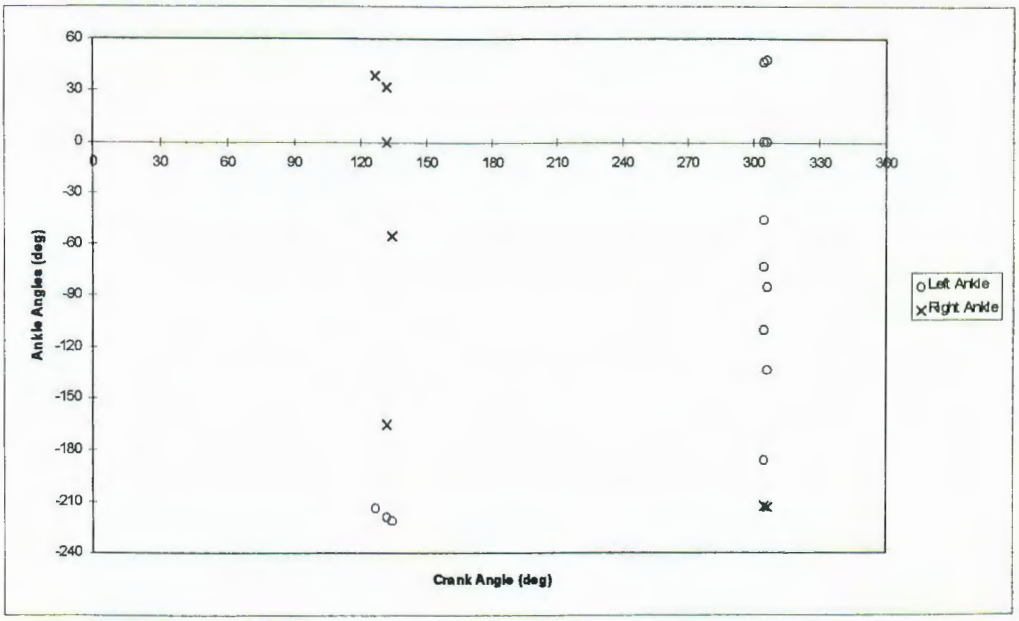

Figure 4.4: Ankle Combinations with Rank(g) < 3, Recumbent Cycling

4.4.2 Optimization of Ankle Angle

Given the fixed ankle strategy for feedback linearization, we can find a more desirable ankle angle by computing the overall effort required to drive the cycle as

$$\int_{t_0}^{t_1} u^2 dt = \int_{t_0}^{t_1} (u_{al}^2 + u_{ar}^2 + u_{hl}^2 + u_{hr}^2 + u_{kl}^2 + u_{kr}^2) dt$$
$$\theta_4(t_1) = \theta_4(t_0) + 2\pi$$

for various ankle angles. Figure 4.5 shows the results over the physical ranges of the ankle angle for recumbent cycling, with the left and right ankles controlled to the same angle. The acceleration constant K4c set to 10 to achieve a full rotation of the crank in a realistic time (1.2 sec), and to allow direct comparison of Figure 4.5 with Figure 3.8 and Figure 3.10. Figure 4.5 clearly shows that certain ankle angles will achieve full rotation of the crank at a lower cost in input effort; in this case, the ideal ankle angle would be approximately 45°. Thus, the foot would remain

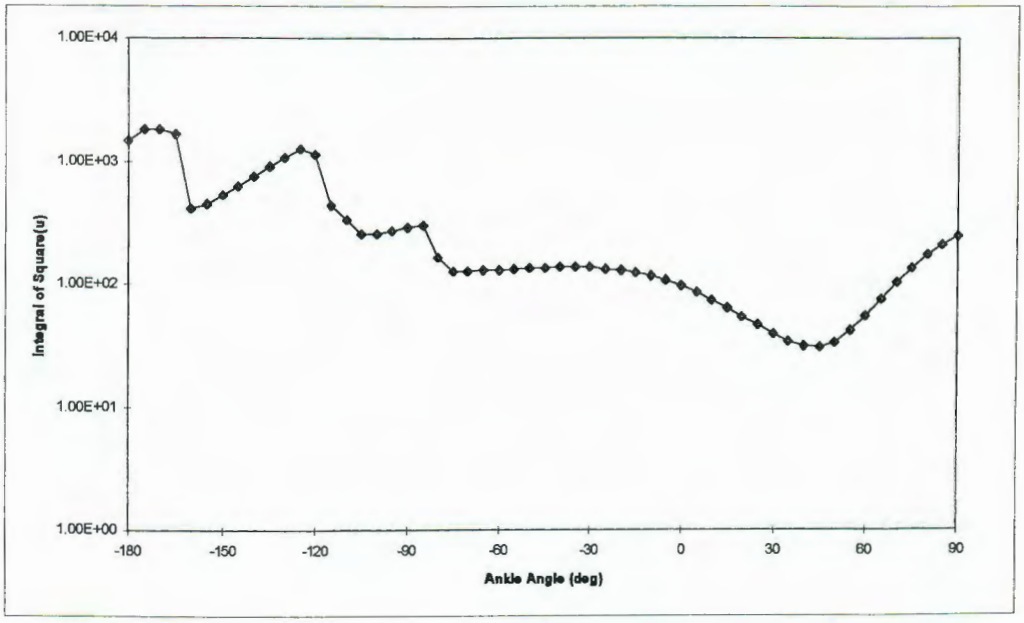

Figure 4.5: Input Effort Required to Complete a Full Cycle vs. Fixed Ankle Angle, Recumbent Cycling

below the horizontal, and would remain near its maximum extent relative to the calf.

4.5 Conclusions

In this chapter, the problem of controlling the Three Degree-of-Freedom model for forward cycling in a recumbent position has been examined. In determining the physical range of motion for the foot, it was shown that the foot is generally freer to move above the horizontal for recumbent cycling, and that the range of motion is not the same for all possible crank angles. Next, following the analysis of Chapter 3, the g-functions of the Three Degree-of-Freedom model were analyzed in detail, and areas where loss of ankle control could occur were shown

not to exist. Feedback linearization was used to "reverse engineer" the desired crank and ankle dynamics and compute the inputs required to achieve the desired dynamics; in this analysis, constant acceleration of the crank. Subrank conditions in the g matrix, the result of unfavorable limb alignments, were identified and shown to be outside the physical range of the ankle angle. Throughout this chapter, it became clear that less effort is required to propel the cycle in the recumbent position than in the upright position given an equal seat-crank distance d, since unfavorable alignments are encountered less often than in the upright position.

Chapter 5 Conclusions and Future Research

In this thesis, dynamic models for human skeletal systems pedaling a bicycle have been used to study several aspects of controlling the cycling. First, the physiological basis for modeling locomotive behavior with control systems techniques was presented. Next, controlling the one degree-of-freedom model was studied. It was demonstrated that successively complex optimization problems could be formulated and solved, with successively better results. This serves as a model for learning locomotive behavior, in that the behavior is simple at first but can be improved through increasingly complex coordination of the limbs.

Next, control strategies for the three degree-of-freedom model were examined. The significant effects of the ankle angles on the rest of the model's dynamics led us to utilize a fixed-ankle strategy. Through analysis of the physical limits of the foot and the dynamics equations, regions can be identified in which the foot should be constrained for effective cycling. Feedback linearization was used to show the ideal input torque profile for achieving a constant acceleration, and for identifying the ankle angle resulting in the minimal effort to complete a full cycle. Additionally, the feedback linearization analysis provided a method for identifying regions of unfavorable limb alignment for a particular set of cyclist parameters, and it was shown that adjustment of the seat height provides a method for avoiding these alignments. Finally, results were developed for recumbent cycling and compared to upright cycling.

The work presented here could be extended in several directions. First, optimization problems with different goals, such as achieving constant velocity, could be examined for the one degree-of-freedom model. Additional steps in the learning process could be added by developing more state and input conditions. Finally, the signals required to drive the cycle could be implemented through the use of Fourier or power series. For the more complex three degree-of-freedom model, additional optimization goals could be examined, such as constant velocity. Feedback linearization was shown to be an effective tool for developing input torques to achieve specific state dynamics; the results of such computations could be used to parameterize "ideal" input torques for implementation through Fourier or power series which would provide a model for construction of muscle signals in the spinal cord.

Appendix A Cycling Modeling Parameters

A.1 Cyclist Parameters

Table A.1 lists the physical quantities used to model the cyclist's limbs for both the three degree-of-freedom model and the one-degree-of-freedom model. Figures 1.2 and 1.3 in Chapter 1 show how the limbs are arranged geometrically. The values in Table A.1 were obtained through the author's crude attempt to measure himself and his red Giant Rincon mountain bicycle.

Table A.1: Physical Parameters for Model Limbs

Component	Limb	Length (m)	Mass (kg)	Radius (m)
1	Thigh	0.40	2.83	0.07
2	Calf	0.45	2.77	0.05
3	Foot (Ankle to Pedal)	0.21	1.82	0.04
4	Foot (Toe to pedal)	0.07	0.64	0.04
5	Crank Arm	0.17	1.70	0.01

Inertia terms were computed as

$$I_n = \tfrac{1}{12} m_n (3r_n^2 + l_n^2)$$

The input torques (in Nm) used for the One Degree-of-Freedom model were as follows:

$$U_{hl_{\min}} = -20 \quad U_{hl_{\max}} = +20$$
$$U_{hr_{\min}} = -20 \quad U_{hr_{\max}} = +20$$
$$U_{kl_{\min}} = -20 \quad U_{kl_{\max}} = +20$$
$$U_{kr_{\min}} = -20 \quad U_{kr_{\max}} = +20$$

The input torques (in Nm) used for the Three Degree-of-Freedom model were as follows:

$$U_{hl_{min}} = -10 \quad U_{hl_{max}} = +10$$
$$U_{hr_{min}} = -10 \quad U_{hr_{max}} = +10$$
$$U_{kl_{min}} = -10 \quad U_{kl_{max}} = +10$$
$$U_{kr_{min}} = -10 \quad U_{kr_{max}} = +10$$

A.2 Bicycle Parameters

The position of the seat of the bicycle is characterized by d, the distance from the crank center to the hip, and η, the angle between HC and the vertical intersecting the crank center (see Chapter 1, Figure 1.2). The lengths were computed as follows:

$$d = 0.60 \text{ m}$$
$$h = d\sin(\xi)$$
$$l = d\cos(\xi)$$

The seat angles used to model upright and recumbent cycling are shown in Table A.2.

Table A.2: Seat Position Angles

Position	η	ξ
Upright	5°	85°
Recumbent	70°	20°

A.3 Angle Conventions

The crank angle θ_4 is referenced to the position of the crank arm attached to the left foot. The right foot is attached to the opposite crank arm, which is 180°

from the left crank arm. Hence, the right foot is always 180° from the left foot. The convention for measuring θ_1 , θ_2 , and θ_4 is the same as in Reference 6 - viewing the left side of the cycle, these angles rotate in a counter-clockwise manner for forward rotation of the crank, and zero corresponds to the "3 o'clock" position. Other authors use the notation TDC for top dead center and BDC for bottom dead center to describe the position of the crank. Top dead center corresponds to the maximal elevation of the pedal, and bottom dead center corresponds to the minimal elevation of the pedal. In the convention used here, left TDC corresponds to a crank angle of 90°, and left BDC corresponds to a crank angle of 270°.

The ankle angles θ_3 and θ'_3 are measured on a set of axes rotated 180 from the axes used for the other joint angles. Thus, an ankle angle of zero corresponds to the foot in a position level to the horizontal with the toes pointing left. A positive ankle angle indicates that the ankle is higher in elevation than the toes, and a negative ankle angle indicates that the toes are higher in elevation than the ankle. Referring to θ_3 as the ankle angle is a bit of a misnomer, since it is really the angle of the foot relative to the horizontal. However, to maintain consistency, the terminology of Reference 6 is used.

Appendix B MATLAB Program Listings

This appendix provides listings of several of the MATLAB programs used to generate the computational results presented in Chapters 2, 3, and 4 of this thesis. The following program listings are provided:

Listing	Program Name	Function
B.1	cyclist.m	Cyclist and bicycle physical paramters
B.2	model1.m	One degree-of-freedom state vector computation
B.3	model0.m	Three degree-of-freedom state vector computation
B.4	h_func.m	Computes h-functions for three DOF model
B.5	theta.m	Computes hip (θ_1) and calf (θ_2) angles from crank angle (θ_4) and ankle angle (θ_3)

B.1 CYCLIST.M

```
% This file sets up the cyclist & cycle parameters
global l1 l2 l3 l4 l5
global r1 r2 r3 r4 r5
global m1 m2 m3 m4 m5
global eta zeta
global d h l I1 I2 I3 I4 I5 If
global l11 l21 l31 l41 l51
global l12 l22 l32 l42 l52
global g Khat1 Khat2
global K1 K2 C

l1 = 0.45;
l2 = 0.40;
l3 = 0.19;
l4 = 0.07;
l5 = 0.17;
r1 = 0.07;
r2 = 0.05;
r3 = 0.04;
r4 = 0.04;
r5 = 0.01;
m1 = 2.83;
m2 = 2.77;
```

```
m3 = 1.81;
m4 = 0.63;
m5 = 1.70;
eta = -5.0*(pi/180);
zeta = 85.0*(pi/180);
d = 0.60;
h = d*sin(zeta);
l = d*cos(zeta);
I1 = (1/12)*m1*((3*r1*r1)+(l1*l1));
I2 = (1/12)*m2*((3*r2*r2)+(l2*l2));
I3 = (1/12)*m3*((3*r3*r3)+(l3*l3));
I4 = (1/12)*m4*((3*r4*r4)+(l4*l4));
I5 = (1/12)*m5*((3*r5*r5)+(l5*l5));
If = (1/12)*mf*((3*rf*rf)+(lf*lf));

l11 = l1/2;
l12 = l1/2;
l21 = l2/2;
l22 = l2/2;
l31 = l3/1;
l32 = l3/2;
l41 = l4/1;
l42 = l4/2;
l51 = l5/1;
l52 = l5/2;
g = 9.8;
% end of cyclist.m
```

B.2 MODEL1.M

```
function xdot = model1(t,x)
%
% state space representation:
% x(1)    = theta (crank angle)
% x(2)    = dtheta = omega (crank velocity)
% xdot(1) = dtheta = x(2) = omega
% xdot(2) = ddtheta (crank acceleration)
% x(3)     = switch
%
global m1 m2 m3 m4 m5
global l1 l2 l3 l4 l5
global l11 l12 l21 l22 l31 l32 l41 l42 l51 l52
global I1 I2 I3
global g eta zeta d h l

ud = 0;
xdot = zeros(2,1);
theta4 = x(1);

theta1 = Theta1(x(1));
theta2 = Theta2(x(1));
theta1p = Theta1(x(1)+pi);
theta2p = Theta2(x(1)+pi);
```

```
f1  = (l5*sin(theta4-theta2))/(l1*sin(theta2-theta1));
f1p = (l5*sin(theta4+pi-theta2p))/(l1*sin(theta2p-theta1p));
f2  = (l5*sin(theta1-theta4))/(l2*sin(theta2-theta1));
f2p = (l5*sin(theta1p-(theta4+pi)))/(l2*sin(theta2p-theta1p));

z1  = cos(theta4-theta2)/sin(theta2-theta1);
z2  = sin(theta4-theta2)*cos(theta2-theta1)/sin(theta2-theta1).^2;
pf1 = (l5/l1)*(z1*(1-f2) - z2*(f2-f1));

z1p  = cos(theta4+pi-theta2p)/sin(theta2-theta1p);
z2p  = sin(theta4+pi-theta2p)*cos(theta2p-theta1p)/sin(theta2p-theta1p).^2;
pf1p = (l5/l1)*(z1p*(1-f2p) - z2p*(f2p-f1p));

y1 = cos(theta1-theta4)/sin(theta2-theta1);
y2 = sin(theta4-theta1)*cos(theta2-theta1)/sin(theta2-theta1).^2;
pf2 = (l5/l2)*(y1*(f1-1) + y2*(f2-f1));

y1p = cos(theta1p-(theta4+pi))/sin(theta2p-theta1p);
y2p = sin(theta4+pi-theta1p)*cos(theta2p-theta1p)/sin(theta2p-theta1p).^2;
pf2p = (l5/l2)*(y1p*(f1p-1) + y2p*(f2p-f1p));

h1l = (m1*l11*l11*f1*f1);
h1l = h1l + m2*((l5*l5)+(l22*l22*f2*f2)+(2*l22*l5*cos(theta4-theta2)*f2));
h1l = h1l + (m3*l52*l52)+(I1*f1*f1)+(I2*f2*f2)+I3;

h1r = (m1*l11*l11*f1*f1);
h1r = h1r + m2*((l5*l5)+(l22*l22*f2p*f2p)+(2*l22*l5*cos(theta4+pi-theta2p)*f2p))
;
h1r = h1r + (m3*l52*l52)+(I1*f1p*f1p)+(I2*f2p*f2p)+I3;

h2l = (I1+m1*l11*l11)*f1*pf1 + (I2+m2*l22*l22)*f2*pf2;
h2l = h2l + m2*l22*l5*(cos(theta4-theta2)*pf2 - sin(theta4-theta2)*(1-f2)*f2);
h2r= (I1+m1*l11*l11)*f1p*pf1p+ (I2+m2*l22*l22)*f2p*pf2p;
h2r = h2r + m2*l22*l5*(cos(theta4+pi-theta2p)*pf2p - sin(theta4+pi-theta2p)*(1-f
2p)*f2p);

h3l = m1*l11*f1*cos(theta1) - m2*l5*cos(theta4)-m2*l22*cos(theta2)*f2;
h3l = g*(h3l - m3*l52*cos(theta4));
h3r = m1*l11*f1p*cos(theta1p) - m2*l5*cos(theta4+pi)-m2*l22*cos(theta2p)*f2p;
h3r = g*(h3r - m3*l52*cos(theta4+pi));

h4l = f1;
h4r = f1p;

h5l = d*l5*cos(theta4-eta)/(l1*l2*sin(theta1-theta2));
h5r = d*l5*cos(theta4+pi-eta)/(l1*l2*sin(theta1p-theta2p));

u = U_ts(x(1),x(3));

xdot(1) = x(2);
xdot(2) =          (h2l+h2r)*x(2).^2;
xdot(2) = xdot(2) +(h3l+h3r);
xdot(2) = xdot(2) + h4l*u(1) + h4r*u(2);
```

```
xdot(2) = xdot(2) + h5l*u(3) + h5r*u(4);
xdot(2) = (xdot(2) - ud)*(1/(h1l+h1r));
xdot(3) = 0;
```

B.3 MODEL0.M

```
function xdot = model0_fl(t,x)

%     x(1) = theta3
%     x(2) = dtheta3
%     x(3) = theta4
%     x(4) = dtheta4
%     x(5) = theta3'
%     x(6) = dtheta3'
%     x(7) = theta4'
%     x(8) = dtheta4'

global Kv31  Kv32 Kv33
global Kv3p1 Kv3p2 Kv3p3
global Kv41  Kv42 Kv43
global uD

% compute f's

        y = h_func(x(1:4));
        h1 = y(:,1);
        h2 = y(:,2);

        yd = h_func(x(5:8));
        h1d = yd(:,1);
        h2d = yd(:,2);

        h11 = h1(1);
        h12 = h1(2);
        h13 = h1(3);
        h14 = h1(4);
        h15 = h1(5);
        h16 = h1(6);
        h17 = h1(7);
        h18 = h1(8);
        h19 = h1(9);
        h21 = h2(1);
        h22 = h2(2);
        h23 = h2(3);
        h24 = h2(4);
        h25 = h2(5);
        h26 = h2(6);
        h27 = h2(7);
        h28 = h2(8);
        h29 = h2(9);
```

```
        j11 = h1d(1);
        j12 = h1d(2);
        j13 = h1d(3);
        j14 = h1d(4);
        j15 = h1d(5);
        j16 = h1d(6);
        j17 = h1d(7);
        j18 = h1d(8);
        j19 = h1d(9);
        j21 = h2d(1);
        j22 = h2d(2);
        j23 = h2d(3);
        j24 = h2d(4);
        j25 = h2d(5);
        j26 = h2d(6);
        j27 = h2d(7);
        j28 = h2d(8);
        j29 = h2d(9);

        den = -(h12*h21*j11) + h11*h22*j11 - h11*j12*j21 +h11*j11*j22;
        if den == 0.0
                den = 0.0001;
        end;

        Q3  = h13*x(2).^2 + h14*x(4).^2 + h15*x(2)*x(4);
        Q3p = j13*x(6).^2 + j14*x(4).^2 + j15*x(6)*x(4);
        Q4  = h23*x(2).^2 + j23*x(6).^2 + (h24+j24)*x(4).^2;
        Q4 = Q4 + (h25*x(2)+j25*x(6))*x(4);

        f3n = (-h12*h21*j11*Q3-h11*h12*j21*Q3p+h11*h12*j11*Q4+h11*h12*j11*uD);
        f3  = (-Q3/h11) + (f3n)/(h11*den);


        f3pn = (-j11*h21*j12*Q3-h11*j12*j21*Q3p+j11*h11*j12*Q4+j11*h11*j12*uD);
        f3p = (-Q3p/j11)+ (f3pn)/(j11*den);

        f4  = (h21*j11*Q3+h11*j21*Q3p-h11*j11*Q4-h11*j11*uD)/den;

        v3  = Kv31*x(1) + Kv32*x(2) + Kv33;
        v4  = Kv41*x(3) + Kv42*x(4) + Kv43;
        v3p = Kv3p1*x(5) + Kv3p2*x(6) + Kv3p3;

        fv = [f3 f3p f4]';
        vv = [v3 v3p v4]';

% compute g's

        g3_al = (h19*h22*j11 - h12*h29*j11 - h19*j12*j21 + h19*j11*j22)/(den);
        g3_ar = -(h12*(-(j19*j21) + j11*j29))/(den);
        g3_hl = (h17*h22*j11 - h12*h27*j11 - h17*j12*j21 + h17*j11*j22)/(den);
        g3_hr = -(h12*(-(j17*j21) + j11*j27))/(den);
        g3_kl = (h18*h22*j11 - h12*h28*j11 - h18*j12*j21 + h18*j11*j22)/(den);
        g3_kr = -(h12*(-(j18*j21) + j11*j28))/(den);
```

```
g3p_al = ((h19*h21 - h11*h29)*j12)/(den);
g3p_ar = (-(h12*h21*j19) + h11*h22*j19 + h11*j19*j22 - h11*j12*j29)/(den);
g3p_hl = ((h17*h21 - h11*h27)*j12)/(den);
g3p_hr = (-(h12*h21*j17)+h11*h22*j17 + h11*j17*j22 - h11*j12*j27)/(den);
g3p_kl = ((h18*h21 - h11*h28)*j12)/(den);
g3p_kr = (-(h12*h21*j18) + h11*h22*j18 + h11*j18*j22 - h11*j12*j28)/(den);

g4_al = ((-(h19*h21) + h11*h29)*j11)/(den);
g4_ar = (h11*(-(j19*j21) + j11*j29))/(den);
g4_hl = ((-(h17*h21) + h11*h27)*j11)/(den);
g4_hr = (h11*(-(j17*j21) + j11*j27))/(den);
g4_kl = ((-(h18*h21) + h11*h28)*j11)/(den);
g4_kr = (h11*(-(j18*j21) + j11*j28))/(den);

v_g3  = [g3_al g3_ar g3_hl g3_hr g3_kl g3_kr];
v_g3p = [g3p_al g3p_ar g3p_hl g3p_hr g3p_kl g3p_kr];
v_g4  = [g4_al g4_ar g4_hl g4_hr g4_kl g4_kr];

gv = [v_g3; v_g3p; v_g4];

uv = U_fl(fv,gv,vv);

xdt = fv + gv*uv;

xdot(1) = x(2);
xdot(3) = x(4);
xdot(5) = x(6);
xdot(7) = x(8);

xdot(2) = xdt(1);
xdot(4) = xdt(3);
xdot(6) = xdt(2);
xdot(8) = xdt(3);
% return
```

B.4 H_FUNC.M

```
function y = h_func(x)
% computes the h functions for model 0
global l1 l2 l3 l4 l5
global r1 r2 r3 r4 r5
global m1 m2 m3 m4 m5
global eta zeta
global d h l I1 I2 I3 I4 I5
global l11 l21 l31 l41 l51
global l12 l22 l32 l42 l52
global g Khat1 Khat2
global K1 K2 C

% x(1) = theta3
% x(2) = dtheta3
% x(3) = theta4
```

```
% x(4) = dtheta4
% h1 = [h11 h12 h13 h14 h15 h16 h17 h18 h19]'
% h2 = [h21 h22 h23 h24 h25 h26 h17 h18 h19]'
h1 = zeros(9,1);
h2 = zeros(9,1);

y = Theta(x(1),x(3));
theta1 = y(1);
theta2 = y(2);

F11 = (l3*sin(theta2-x(1)))/(l1*sin(theta1-theta2));
F12 = (l5*sin(theta2-x(3)))/(l1*sin(theta1-theta2));
F21 = (l3*sin(x(1)-theta1))/(l2*sin(theta1-theta2));
F22 = (l5*sin(x(3)-theta1))/(l2*sin(theta1-theta2));

t1 = I1 + m1*l11.^2;
t2 = I2 + m2*l22.^2;
t3 = I3 + I4 + m2*l3.^2 + m3*l32.^2 + m4*l41.^2;
t4 = I5 + m3*l52.^2 + (m2+m3+m4)*l5.^2;
t5 = 2*l22*l3*m2;
t6 = 2*l22*l5*m2;
t7 = 2*l5*(m2*l3 + m3*l32-m4*l41);
t8 = m1*g*l11;
t9 = m2*g*l22;
t10 = (m2*l3+m3*l32-m4*l41)*g;
t11 = (m2+m3+m4)*g*l5+m5*g*l52;
t12 = (m2+m3+m4+m5)*g*h;

A = t1*F11.^2 + t2*F21.^2 + t3 + t5*cos(x(1)-theta2)*F21;
B = 2*t1*F11*F12 + 2*t2*F21*F22 + t5*cos(x(1)-theta2)*F22;
B = B + t6*cos(x(3)-theta2)*F21 + t7*cos(x(3)-x(1));
C = t1*F12.^2 + t2*F22.^2 + t4 + t6*cos(x(3)-theta2)*F22;

R1 = 2*t2*F21+t6*cos(x(1)-theta2);
R2 = 2*t2*F22+t6*cos(x(1)-theta2);
S1 = 1/(sin(theta1-theta2));
S2 = cos(theta1-theta2)/(sin(theta1-theta2).^2);

dF11dt3 = (cos(theta2-x(1))*S1*(F21-1)-sin(theta2-x(1))*S2*(F11-F21));
dF11dt3 = dF11dt3*(l3/l1);
dF11dt4 = (cos(theta2-x(1))*S1*(F22-1)-sin(theta2-x(1))*S2*(F12-F22));
dF11dt4 = dF11dt4*(l3/l1);

dF12dt3 = (cos(theta2-x(3))*S1*(F21-1)-sin(theta2-x(3))*S2*(F11-F21));
dF12dt3 = dF12dt3*(l5/l1);
dF12dt4 = (cos(theta2-x(1))*S1*(F22-1)-sin(theta2-x(1))*S2*(F12-F22));
dF12dt4 = dF12dt4*(l5/l1);

dF21dt3 = (cos(x(1)-theta1)*S1*(1-F11)-sin(x(1)-theta1)*S2*(F11-F21));
dF21dt3 = dF21dt3*(l3/l1);
dF21dt4 = (cos(x(1)-theta1)*S1*(-F21)-sin(x(1)-theta1)*S2*(F12-F22));
dF21dt4 = dF21dt4*(l3/l1);

dF22dt3 = (cos(-theta1+x(3))*S1*(-F11)-sin(-theta1+x(3))*S2*(F11-F21));
```

```
dF22dt3 = dF22dt3*(l5/l1);
dF22dt4 = (cos(-theta1+x(3))*S1*(1-F12)-sin(-theta1+x(3))*S2*(F12-F22));
dF22dt4 = dF22dt4*(l5/l1);

dAdt3 = 2*t1*F11*dF11dt3 + R1*dF21dt3 - t5*sin(x(1)-theta2)*(1-F21)*F21;
dAdt4 = 2*t1*F11*dF11dt4 + R1*dF21dt4 - t5*sin(x(1)-theta2)*(-F22)*F21;
dBdt3 = R1*dF22dt3 + R2*dF21dt3 + 2*t1*(F12*dF11dt3 + F11*dF12dt3);
dBdt3 = dBdt3 - t5*sin(x(1)-theta2)*(1-F21)*F22;
dBdt3 = dBdt3 - t6*sin(x(3)-theta2)*(-F22)*F21;
dBdt4 = R1*dF22dt4 + R2*dF21dt4 + 2*t1*(F12*dF11dt4+F11*dF12dt4);
dBdt4 = dBdt4 - t5*sin(x(1)-theta2)*(-F22)*F22;
dBdt4 = dBdt4 - t6*sin(x(3)-theta2)*(1-F22)*F21;
dCdt3 = 2*t1*F12*dF12dt3 + R2*dF22dt3-t5*sin(x(1)-theta2)*(1-F22)*F21;
dCdt4 = 2*t1*F12*dF12dt4 + R2*dF22dt4-t5*sin(x(1)-theta2)*(1-F22)*F22;

h11 = A;
h12 = B/2;
h13 = dAdt3/2;
h14 = (dBdt4 - dCdt3)/2;
h15 = dAdt4;
h16 = -t8*cos(theta1)*F11 + t9*cos(theta2)*F21 + t10*cos(x(1));
h17 = F11;
h18 = F11 - F12;
h19 = 1-F21;
h21 = B/2;
h22 = C;
h23 = (dBdt3 - dAdt4)/2;
h24 = dCdt3/2;
h25 = dCdt3;
h26 = -t8*cos(theta1)*F12 + t9*cos(theta2)*F22 + t11*cos(x(3));
h27 = F12;
h28 = F12 - F22;
h29 = -F22;
h1 = [h11 h12 h13 h14 h15 h16 h17 h18 h19]';
h2 = [h21 h22 h23 h24 h25 h26 h27 h28 h29]';
y = [h1 h2];
% end of h_func.m
```

B.5 THETA.M

```
function y = Theta(theta3,theta4,params)
%
AC2 = l3*l3 + l5*l5 - 2*l3*l5*cos(pi-theta4+theta3);
AC = (AC2).^(0.5);
cthetah = (l3*cos(theta3) + l5*cos(theta4))/AC;
sthetah = (l3*sin(theta3) + l5*sin(theta4))/AC;
thetah = atan2(sthetah,cthetah);
AH2 = (d.^2) + AC2 - 2*d*AC*sin(thetah+eta);
AH = sqrt(AH2);
cy = (d-AC*sin(thetah+eta))/(AH);
sy = -(AC/AH)*(cos(thetah)+eta);
cx = (AH2 + l1.^2-l2.^2)/(2*AH*l1);
```

```
sx = sqrt(1-cx.^2);
cw = (AH2 + l2.^2-l1.^2)/(2*AH*l2);
sw = sqrt(1-cw.^2);
cz = (AC-d*sin(thetah+eta))/(AH);
sz = -(d/AH)*cos(thetah+eta);
x = atan2(sx,cx);
y = atan2(sy,cy);
w = atan2(sw,cw);
z = atan2(sz,cz);
st1 = sin(zeta - x - y);
ct1 = cos(zeta - x - y);
st2 = sin(-pi + w + z + thetah);
ct2 = cos(-pi + w + z + thetah);
t1 = atan2(st1,ct1);
t2 = atan2(st2,ct2);
if (t2 < 0.0)
        t2 = 2*pi+t2;
end
y = [t1 t2];
```

Appendix C Correction to Time Optimal Bang-Bang Input Results

There is an inaccuracy in Reference 6 which leads to an error in the analytic results for the time optimal control problem for the one degree-of-freedom model. The dynamics for the model are presented in Chapter 2, section 2.3 of Reference 6. The following angles are used: θ_1 is the hip angle, θ_2 is the calf angle, and θ_4 is the crank angle. The dynamics are represented by the following equation:

$$\begin{aligned}&\left(h_1(\theta_4)+h_1(\theta_4+\pi)\right)\ddot{\theta}_4-\left(h_2(\theta_4)+h_2(\theta_4+\pi)\right)\dot{\theta}_4^2-\left(h_3(\theta_4)+h_3(\theta_4+\pi)\right)\\&\quad=h_4(\theta_4)u_{hl}+h_4(\theta_4+\pi)u_{hr}+h_5(\theta_4)u_{kl}+h_5(\theta_4+\pi)u_{kr}-u_D\end{aligned}$$

where

$$h_4(\theta_4)=\frac{l_5\sin(\theta_4-\theta_2)}{l_1\sin(\theta_2-\theta_1)},\quad h_5(\theta_4)=\frac{dl_5\cos(\theta_4-\eta)}{l_1l_2(\theta_2-\theta_1)}$$

On page 23 of Reference 6, the author states that

$$\angle KAC=\begin{cases}\pi-\theta_4+\theta_2 & \text{when left foot is left of } HC\\(\pi-\theta_2)+(\theta_4-2\pi) & \text{when left foot is right of } HC\end{cases}$$

From Figure 1, HC is defined by η, so the condition for the angle KAC can be restated as

$$\angle KAC=\begin{cases}\pi-\theta_4+\theta_2 & \text{for } \frac{\pi}{2}-\eta\le\theta_4\le\frac{3\pi}{2}-\eta\\(\pi-\theta_2)+(\theta_4-2\pi) & \text{for } \frac{3\pi}{2}-\eta\le\theta_4\le\frac{\pi}{2}-\eta\end{cases}$$

The author then uses this statement to show that

$$h_4(\theta_4)\begin{cases}>0 & \frac{\pi}{2}-\eta<\theta_4<\frac{3\pi}{2}-\eta\\<0 & \frac{3\pi}{2}-\eta<\theta_4<\frac{\pi}{2}-\eta\end{cases}$$

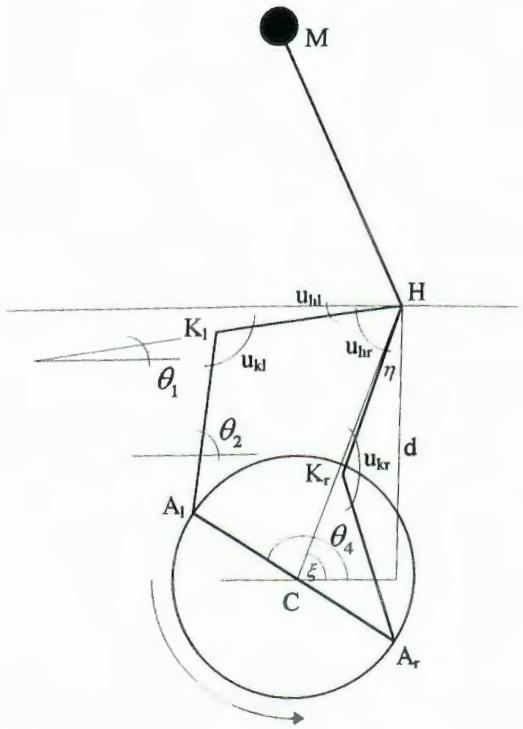

Figure C.1: One Degree-of-Freedom Cycling Model

and then uses this result in section 3.2 and 3.3 of Reference 6 to show that the bang-bang input switchpoints for the hip inputs occur at $\frac{\pi}{2} - \eta$ and $\frac{3\pi}{2} - \eta$. However, this result is not correct, since the interval conditions on *KAC* are incorrect. Since

$$h_4(\theta_4) = \frac{l_5 \sin(\theta_4 - \theta_2)}{l_1 \sin(\theta_2 - \theta_1)}$$

the intervals defining the opposite signs of h_4 are correctly defined by $\theta_4 - \theta_2 = 0, \pi$, which are not coincident with $\theta_4 = \frac{\pi}{2} - \eta, \frac{3\pi}{2} - \eta$ for every set of cyclist parameters. This can be shown by the following geometric argument: Suppose $\theta_4 = \frac{\pi}{2} - \eta$ and $\theta_4 = \theta_2$. Then *K*, *A*, and *C* are colinear in Figure C.1, and

are colinear with HC. The holonomic constraint of equation 2.3.1 in Reference 6 states that

$$l_1 \sin\theta_1 + l_2 \sin\theta_2 + l_5 \sin\theta_4 - h = 0 \quad \forall\theta_4$$

Note that, $\theta_4, \theta_2 = \frac{\pi}{2} - \eta \Rightarrow \theta_1 = \frac{\pi}{2} - \eta$ and $h = d\sin(\frac{\pi}{2} - \eta)$, so the constraint can be restated as

$$\begin{aligned} & l_1 \sin(\tfrac{\pi}{2} - \eta) + l_2 \sin(\tfrac{\pi}{2} - \eta) + l_5 \sin(\tfrac{\pi}{2} - \eta) - d\sin(\tfrac{\pi}{2} - \eta) = 0 \quad \forall\theta_4 \\ & \Rightarrow l_1 + l_2 + l_5 = d \end{aligned}$$

However, if this holds true, then the crank obviously cannot move beyond $\theta_4 = \frac{\pi}{2} - \eta$ since C, A, K, and H are all colinear, and K lies between A and H. Thus,

$$\angle KAC = \begin{cases} \pi - \theta_4 + \theta_2 & \text{for} \frac{\pi}{2} - \eta \le \theta_4 \le \frac{3\pi}{2} - \eta \\ (\pi - \theta_2) + (\theta_4 - 2\pi) & \text{for} \frac{3\pi}{2} - \eta \le \theta_4 \le \frac{\pi}{2} - \eta \end{cases}$$

only holds for a particular, non-realistic set of cyclist parameters and does not apply in the general case. Consequently, the condition

$$h_4(\theta_4) \begin{cases} > 0 & \frac{\pi}{2} - \eta < \theta_4 < \frac{3\pi}{2} - \eta \\ < 0 & \frac{3\pi}{2} - \eta < \theta_4 < \frac{\pi}{2} - \eta \end{cases}$$

should be restated as

$$h_4(\theta_4) \begin{cases} > 0 & \alpha < \theta_4 < \alpha + \pi \\ < 0 & \alpha + \pi < \theta_4 < \alpha + 2\pi \end{cases}$$

where α is such that

$$\theta_2 = \begin{cases} \theta_4 & \text{for } \theta_4 = \alpha \\ \theta_4 - \pi & \text{for } \theta_4 = \alpha + \pi \end{cases}$$

Geometrically, α is the crank angle at which KA and AC are colinear and at which the hip angle θ_l reaches a minimum, and $\alpha+\pi$ is the crank angle at which KA and AC are colinear and the hip angle θ_l reaches a maximum. Carrying this through to the optimal bang-bang input results presented in Chapter 3 of Reference 6, the hip inputs should be switched at α and at $\alpha+\pi$, not at $\frac{\pi}{2}-\eta$ and $\frac{3\pi}{2}-\eta$ as the authorconcluded. This explains why the computational results for separate optimized switches in the hips and knees do not occur at the same angles for the hip and knee. In fact, the computational results show that the hip switchpoints occur at α and at $\alpha+\pi$, not at $\frac{\pi}{2}-\eta$ and $\frac{3\pi}{2}-\eta$, whereas the knee input switchpoints occur at $\frac{\pi}{2}-\eta$ and $\frac{3\pi}{2}-\eta$, since that is where the minimum and maximum knee angles occur.

REFERENCES

[1] Levine & Loeb, "Neural Control of Limb Movement", *IEEE Control Systems Magazine*, pp. 38-47, December 1992.

[2] E. Sim, B. Ma, W. Levine, F. Zajac, "Some Results on the Neuromuscular Controls Involved in Pedaling a Bicycle at Maximum Speed", *Proceedings of the 1989 Automatic Control Conference*, 1989.

[3] Shik, M.Ll, Orlovskii, G.N., Severin, F.V. (1966) "Locomotion of the mesencephalic cat evoked by pyramidal stimulation",*Biofizika*, 13(1):127-135.

[4] Armstrong, D.M. (1988), "The Supraspinal Control of Mammalian Locomotion," *Journal of Physiology*, 405, pp. 1-37.

[5] Newell, K.M., McDonald, P.V., and Kugler, P.N., (1991) "The Perceptual-Motor Workspace and the Acquisition of Skill,", *Proceedings of the NATO Advanced Study Institute on Tutorials in Motor Neuroscience*, Kluwer Academic Publishers, The Netherlands.

[6] Ma, Baoming, "The Dynamics and Time Optimal Control for the Skeletal System of Humans Pedaling a Stationary Bicycle", *M.S. Thesis*, University of Maryland, 1989.

[7] Sim, Eunsup, "The Application of Optimal Control Theory for Analysis of Human Jumping and Pedaling", *Ph.D. Dissertation*, University of Maryland, 1988.

[8] Whitt, Frank Rowland, *Bicycling Science*, (Cambridge, MA: MIT Press, 1982), pp. 53.

[9] Burke, Edmund R., *Science of Cycling*, (Chicago: Human Kinetics Publishers, Inc., 1986).

[10] Kailath, Thomas, Linear Systems, (Englewood Cliffs, NJ: Prentice-Hall, Inc., 1980), pp. 667-8.